

Deliverable D.T. 4.1.1

Data collection, modelling and prediction

Erpicum, Sébastien; Bennet, Loïc; Burghardt, Lisa; Klopries, Elena-Maria; Poppema, Daan W.; Wüthrich, Davide

Publication date

2023

Document Version

Final published version

Citation (APA)

Erpicum, S., Bennet, L., Burghardt, L., Klopries, E.-M., Poppema, D. W., & Wüthrich, D. (2023). *Deliverable D.T. 4.1.1: Data collection, modelling and prediction*. EMfloodResilience Consortium.
https://emfloodresilience.eu/publish/pages/7427/2023-12-11_report_emfloodresilience_d-4-1-1.pdf

Important note

To cite this publication, please use the final published version (if applicable).
Please check the document version above.

Copyright

Other than for strictly personal use, it is not permitted to download, forward or distribute the text or part of it, without the consent of the author(s) and/or copyright holder(s), unless the work is under an open content license such as Creative Commons.

Takedown policy

Please contact us and provide details if you believe this document breaches copyrights.
We will remove access to the work immediately and investigate your claim.

DELIVERABLE D.T4.1.1

Data collection, modelling and prediction

EMfloodResilience

INTERREG Euregio Maas-Rijn | Project No. EMR228

The EMfloodResilience project is being carried out within the context of Interreg V-A Euregio MeuseRhine and is 90% funded from the European Regional Development Fund.

Dissemination level	Public
Type of deliverable	Report
Work package	WP4
Deliverable number	D.T4.1.1
Status - version, date	Final - V1.0, 11/12/2023
Deliverable leader	University of Liège Dr. ir. Sébastien Ercicum Loïc Benet
Deliverable contributors	RWTH Aachen University Lisa Burghardt Dr.-Ing. Elena-Maria Klopries Delft University of Technology Dr. ir. Daan W. Poppema Dr. ir. Davide Wüthrich
Contractual date of delivery	31/12/2023
Keywords	Flood damage, clogging, bridges, floating debris, Large Wood

Acknowledgements

We thank Dennis Ronkers, Michiel Hendriks, Ningyi Chen, Ruben Wessendorp (TU Delft), Florence Dütz, Fabrice Hamonou, Gianni Massin, Milly Peyrard (University of Liège) and Mariana Vélez Pérez, Lino Schröter, Mariia Gimelbrant, Ben Lindner and Louisa Blitz (RWTH Aachen) for their assistance in the photo analysis and flume experiments.

Legal Disclaimer

Copyright © EMfloodResilience Consortium, 2023.

Table of contents

List of figures

List of tables

List of abbreviations and acronyms

Executive Summary..... 8

1 Introduction 10

- 1.1 Background and study area 10
- 1.2 Objectives 12
- 1.3 Report outline..... 13
- 1.4 Content..... 13

2 Field data: debris accumulation during the 2021 floods..... 14

- 2.1 Field data: collection methods and database description 14
- 2.2 Field data: results and synthesis 15

3 Experimental modelling 19

- 3.1 Experimental methods and database description 19
 - 3.1.1 Test setup: labs and flumes 20
 - 3.1.2 Test setup: bridges 22
 - 3.1.3 Test setup: debris 24
 - 3.1.4 Test program 25
 - 3.1.5 Database description and encoding 28
- 3.2 Results of experiments and synthesis 29
 - 3.2.1 Debris composition..... 29
 - 3.2.2 Hydraulic conditions and bridge design 30

4 Design recommendations and operational procedures 34

- 4.1 Bridge design 34
- 4.2 Operational procedures and river basin management 35

References

Appendices 39

Appendix 1: Parameter description of field observation database

Appendix 2: Detailed composition of different debris mixtures

Appendix 3: Density measurements for the debris components in wet and dry state

Appendix 4: Overview of all the tests conducted in the three laboratories

List of figures

Figure 1: Bridge affected by floating debris on the Vesdre River at Verviers, Belgium (courtesy J. Mawet)	10
Figure 2: The study Area in Germany, Belgium and the Netherlands.....	12
Figure 3: Structure of the work package depicted in this report	13
Figure 4: Two extreme examples of debris accumulation, with trees, building rubble, caravans, tanks and other materials show the backwater rise caused by accumulations. Location: Kreuzberg, Germany and Pepinster, Belgium.	15
Figure 5: Debris compositions observed from the field data after the flood event 2021. Blue squares in subplot C) and D) indicate debris mixtures studied in the experiments (Chapter 3.1.4).	16
Figure 6: Observed debris volumes, per unit meter width as a factor of span width (pier spacing) and flood height above the river deck. Dashed lines indicate the region where large accumulations are most likely.	17
Figure 7: Modelling Strategy	19
Figure 8: Experimental set-up for the flume B2 in Liège.....	20
Figure 9: Experimental set-up in the flume G1 in Aachen	21
Figure 10: Experimental setup in Delft.....	22
Figure 11: Bridge dimensions for the model scale 1:16. a) Rectangular bridge opening, b) arched opening and c) sideview of the different handrail designs.....	23
Figure 12: Bridge dimensions for the model scale 1:18 with no handrail and the two pier variations.....	23
Figure 13: Debris components	24
<i>Figure 14: Overview over the different bridge designs tested with debris compositions containing 75% of logs and 25% of plates (lower bar) and 25% of cubes (upper bar) in the labs in Aachen (a), Delft (b), Liège flume B1 (c) and Liège flume B2 (d). Different colours indicate different initial water depths, fill patterns bridge designs.</i>	<i>26</i>
Figure 15: Backwater rise for the tests conducted with varying debris compositions in Liège. The initial water depth is 270 mm at a Froude number of 0.28, so e.g. $\Delta H=270$ mm signifies debris doubling the original water depth.	29
Figure 16: Backwater rise for the tests conducted with varying debris compositions in Aachen	30
Figure 17: Relative backwater rise for the experiments conducted with a debris composition of 25% plates and 75% logs and 25% cubes and 75% logs for varying Froude numbers	31

Figure 18: Relative Backwater rise in relation to the initial water depth h_0 for the model in Liège with a scale of 1:18	32
Figure 19: Relative backwater rise for different handrail designs for the tests conducted in the lab in Aachen	32
Figure 20: Relative backwater rise for different handrail designs, compared to a bridge without handrail. Data Delft, $Fr_0=0.15$, h_0 near the top of the handrail. NB: this figure also plots backwater rise by the bridge itself, in all other plots backwater rise purely refers to backwater rise from debris. ...	33
Figure 21: Relative backwater rise for bridges with rectangular and arched opening shape in the flume in Aachen	33

List of tables

Table 1: The debris categories distinguished in the database, and the ratios used to translate this into volume fractions for log-shaped, plate-shaped and cuboid debris.	15
Table 2: Modelling scenarios with different debris compositions	24
Table 3 : The hydraulic conditions and number of repetitions for the experiments conducted at 1 :16 scale in Delft, Liege and Aachen, using a porous handrail and two piers. #/# refers to the number of repetitions with 25% plates resp. 25% cubes and 75% logs, h_0 is the initial water level and Fr_0 the initial Froude number at the beginning of each experiment.....	25
Table 4: The hydraulic conditions and number of repetitions for the conducted experiments at 1 :18 scale in Liège, using two piers, no handrail and rectangular openings. #/# refers to the number of repetitions with 75% logs and 25% plates resp. cubes, h_0 is the initial water level and Fr_0 the initial Froude number at the start of each experiment	26
Table 5: The hydraulic conditions and number of repetitions for the alternative bridge designs tested at 1:16 scale in Aachen and Delft, all with two piers. #/# refers to the number of repetitions with 25% plates resp. 25% cubes and 75% logs.....	27
Table 6 : The hydraulic conditions and number of repetitions for the bridge with one pier tested at 1 :18 scale in Liège (flume B2), without handrail. #/# refers to the number of repetitions with 25% plates resp. 25% cubes and 75% logs	27

List of abbreviations and acronyms

Abbreviation	Meaning
Δh	Backwater rise
h_0	Initial water depth in front of the bridge
h	Flow depth [m]
Fr	Froude number, defined as $Fr = \frac{v}{\sqrt{gh}}$
v	Flow velocity [m/s]
NRW	North Rhine-Westphalia
UDS	Ultrasonic distance sensor for water levels

Executive Summary

In July 2021, an extreme flood occurred in Belgium, The Netherlands and Germany, causing more than 200 casualties and over 30 billion euro of damage to buildings and infrastructure. Numerous river structures were blocked by floating debris, increasing upstream water levels and thereby the extent of flooding. Moreover, debris accumulation frequently caused structural damage at bridges. This event forms both the motivation to study floating debris accumulation better, as well as a unique opportunity to collect invaluable field data, needed to provide a better understanding of the physical processes involved during floods.

In this report, we first present a database of floating debris accumulation during the 2021 floods, documenting the geometry and characteristics of both the affected structures and the debris deposits. The data collection, performed by ULiege, RWTH Aachen and TUDelft teams, focuses on three rivers particularly affected by the flood: the Vesdre in Belgium, the Ahr in Germany and the Geul in The Netherlands. Along these three rivers, photos taken during and directly after the flood have been systematically analysed to identify structures affected by debris deposits, determine deposit dimensions, and classify deposit composition. The location and geometry of affected structures have also been documented, as well as main flow conditions during the event. The resulting database includes 33 bridges in Belgium, 38 bridges in Germany and one culvert in the Netherlands, and encompasses around 60 parameters for each identified structure. It constitutes a unique database that can be used to improve our understanding of debris blockage at structures and to assess the impact of debris blockage on flood conditions. This database first showed the severity of the flood, with peak water levels at the studied bridges reaching more than 1 m above the bridge deck for 40% of the bridges, 13 of the 71 bridges structurally severely damaged and an additional 19 too damaged to be kept in service. Secondly, it showed that the largest debris accumulations occurred at bridges with simultaneously A) a pier spacing of less than 10 meters, allowing large trees to span the distance between piers and B) peak water levels at or above the deck, allowing the deck and railing to block debris. Third, it showed that about 50 percent of the debris volume in both countries consisted of trees. The remainder predominantly consisted of building rubble, construction wood, tanks and, in Germany, cars and caravans.

Based on these data, physical experiments were conducted at all three universities in order to determine how backwater rise (the increase of the upstream water level due to debris blockage) depends on the debris composition, hydraulic conditions and bridge design. For all three aspects, information from the bridge clogging database was used to determine the experimental setup and tested scenarios. The results of the experimental modelling were reported in a second database, which documents more than 280 tests. Results show that the presence of plates (e.g. flat objects) in the debris mixture increases the backwater rise while voluminous objects such as tanks or cars can lead to a less dense accumulation and less backwater rise. For the hydraulic conditions, tests show that the relative backwater rise increases with increasing Froude number and decreases with increasing initial water depth. This is in agreement with previous studies. At last, tests with modified bridge designs show that a reduction of the number of piers reduces the clogging probability. At bridges with no handrail, a lower backwater rise could be observed since the debris could pass the bridge deck sooner.

Based on the observed debris accumulations and experiments, the recommendation for bridge design is to use slimmer bridge decks, large freeboard between bridge deck and water level, implement collapsible or foldable handrails and reduce the number of piers. Regarding operational procedures and flood risk

management, the effect of clogging should be implemented in flood hazard and flood risk maps as well as emergency plans. The effect of clogging at bridges and therefore the risk of damage should be communicated, and measures to reduce the accumulation of debris at bridges should be integrated in the river basin management.

1 Introduction

1.1 Background and study area

In July 2021, several days of heavy rainfall resulted in severe flooding within the Meuse and Rhine river basins in Europe (Mohr et al., 2023; Schäfer et al., 2021). Water levels and inundation areas of the 100-year-flood were far exceeded, leading to around 220 casualties and damages up to 30 billion Euros within the three countries Belgium, Germany and the Netherlands (Koks et al., 2022; Mohr et al., 2023). Many areas of critical infrastructure were directly affected (Korswagen et al., 2022), strongly restricting the first response to the flood event. Even two years after the flood, the reconstruction of roads, bridges, railway and utility networks have not been completed, still hampering the day-to-day life and further reconstructions processes. (Deutsches Komitee Katastrophenvorsorge e.V [DKKV], 2022; Lemnitzer et al., 2023)

The impact of bridges on the flood event 2021 quickly became evident. Large volumes of floating debris accumulated in front of the bridges, leading to increased water levels and therefore a larger extent of the inundated area (see Figure 1). Furthermore, the increased hydraulic loads on the bridge structures and the foundations caused the collapse of several bridges. The waves released by the collapse of bridges were characterized by the transport of debris and high flow velocities and water levels, leading to a higher damage potential. (Burghardt et al., 2022; Tubaldi et al., 2022; Zanke, 2013)

The extreme precipitation and subsequent flooding occurred across all three countries and since the catchment areas exceed the national borders, a transnational cooperation is recommendable. At the bridges, processes of debris clogging, erosion and bridge collapse could be observed which all should be considered in future flood risk assessments. Previous studies on debris accumulations were mainly based on experiments conducted with single piers without bridge deck, or debris racks instead of bridges. Therefore, field observations of bridge clogging during the 2021 flood event can be used to better understand the processes and consequences for actual bridges.

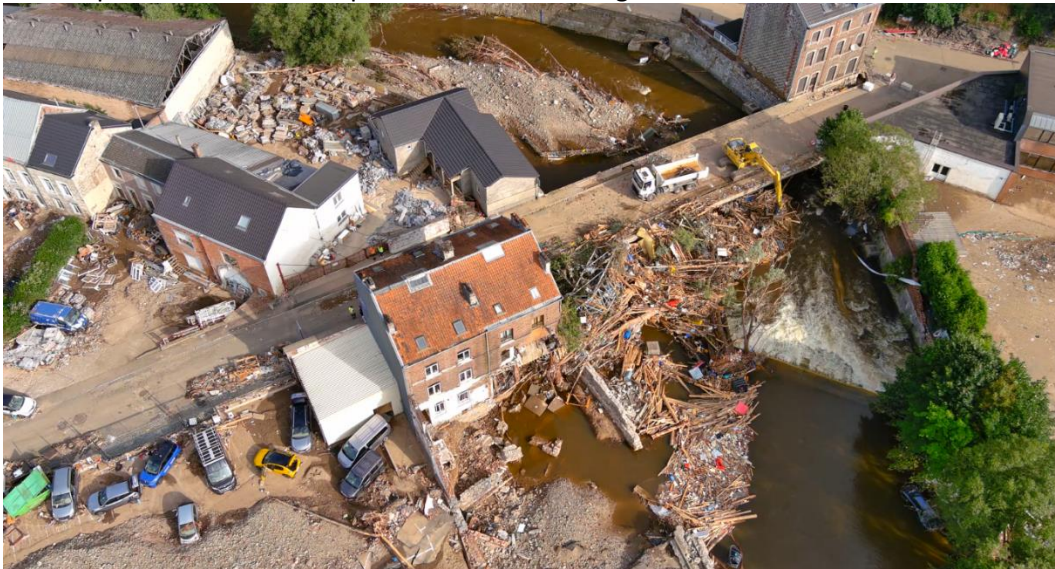


Figure 1: Bridge affected by floating debris on the Vesdre River at Verviers, Belgium (courtesy J. Mawet)

To better understand the debris accumulation process and consequences, debris accumulation at hydraulic structures is studied, with a focus on events during the 2021 flood in the border region of Belgium, Germany and the Netherlands. Within this area, data was collected on clogging of bridges and culverts along the seven most affected rivers: the Ahr, Inde and Vicht in Germany, the Vesdre, Helle and Hoëgne in Belgium and the Geul in the Netherlands (Figure 2). Most of these rivers are part of the Meuse catchment area; only the Ahr is a tributary of the Rhine.

The greatest extent of damage was documented in the German states of Rhineland-Palatinate and North Rhine-Westphalia. Data could be collected here on clogging along the rivers Inde and Vicht, part of the Rur catchment area as well as for the river Ahr (see Figure 2). The Vicht is the second largest tributary of the river Inde with a catchment area of 104 km² (Land NRW, 2023; Wasserverband Eifel-Rur [WVER], n. a.b). The headwaters of the Inde lay in Belgium and it reaches a total length of 47 km (Land NRW, 2023; WVER, n. a.a). About one fifth of the catchment area is classified as heavily modified due to settlement and industrial areas within the cities Eschweiler, Stolberg and Jülich. Both rivers Inde and Vicht are influenced by dams for the purpose of drinking water supply (International Commission on Large Dams, 2013). The 900 km² wide catchment area of the Ahr river lies in the low mountain range of both North Rhine-Westphalia (25%) and Rhineland Palatinate (76%). The Ahr is a tributary of the Rhine with a slope of 0.4% and its valley is characterized by steep hillsides consisting of sand- and siltstone. (Landesamt für Umwelt Rheinland-Pfalz [LfU], n. d.; Ministerium für Klimaschutz, Umwelt, Energie und Mobilität Rheinland-Pfalz [MKUEM], n. d.)

In Belgium, debris accumulation is studied at the river Vesdre, and its tributaries Helle and Hoëgne. The Vesdre (Weser in German) originates in the High Fens plateau in north-eastern Wallonia. After 70 km, near Liege, it joins the Ourthe, i.e. the main Belgian tributary of the Meuse. The Vesdre (also called Eupen) dam (Wesertalspere in German) just before the town of Eupen and the La Gileppe dam regulate discharge from the upstream part of the catchment and provide storage for drinking water. The lower part of the Vesdre catchment is mostly characterized by urban and industrial areas (Bauwens et al., 2011). The Helle (Hill in German) also originates in the High Fens plateau and merges with the Vesdre in Eupen. Upstream of Eupen, a part of the Helle discharge is diverted through a tunnel into the aforementioned Vesdre dam (Bruwier et al., 2015). Lastly, the Hoëgne joins the Vesdre at Pepinster. The Hoëgne is not regulated by reservoirs, leading to periodic flood events (Bruwier et al., 2015). Regarding surface area, the Helle and Hoëgne make up 5% and 30% of the 683 km² Vesdre catchment. Both the Helle and Hoëgne have comparatively steep slopes, of 1.6% and 1.7%.

In the Netherlands, debris accumulation is studied at the river Geul in Limburg. The Geul originates in Belgium, just south of Aachen in the border region with Germany. It flows through the Netherlands for approximately the last two-thirds of its 58 km length, before flowing into the Meuse. It has an average gradient of approximately 0.4%, and a catchment area of 340 km². Near Bunde, flooding occurred, because the submerged culvert that carries the Geul water underneath the Juliana Canal formed a bottleneck. At this culvert, debris accumulation occurred, further reducing its capacity and thus increasing upstream flooding.

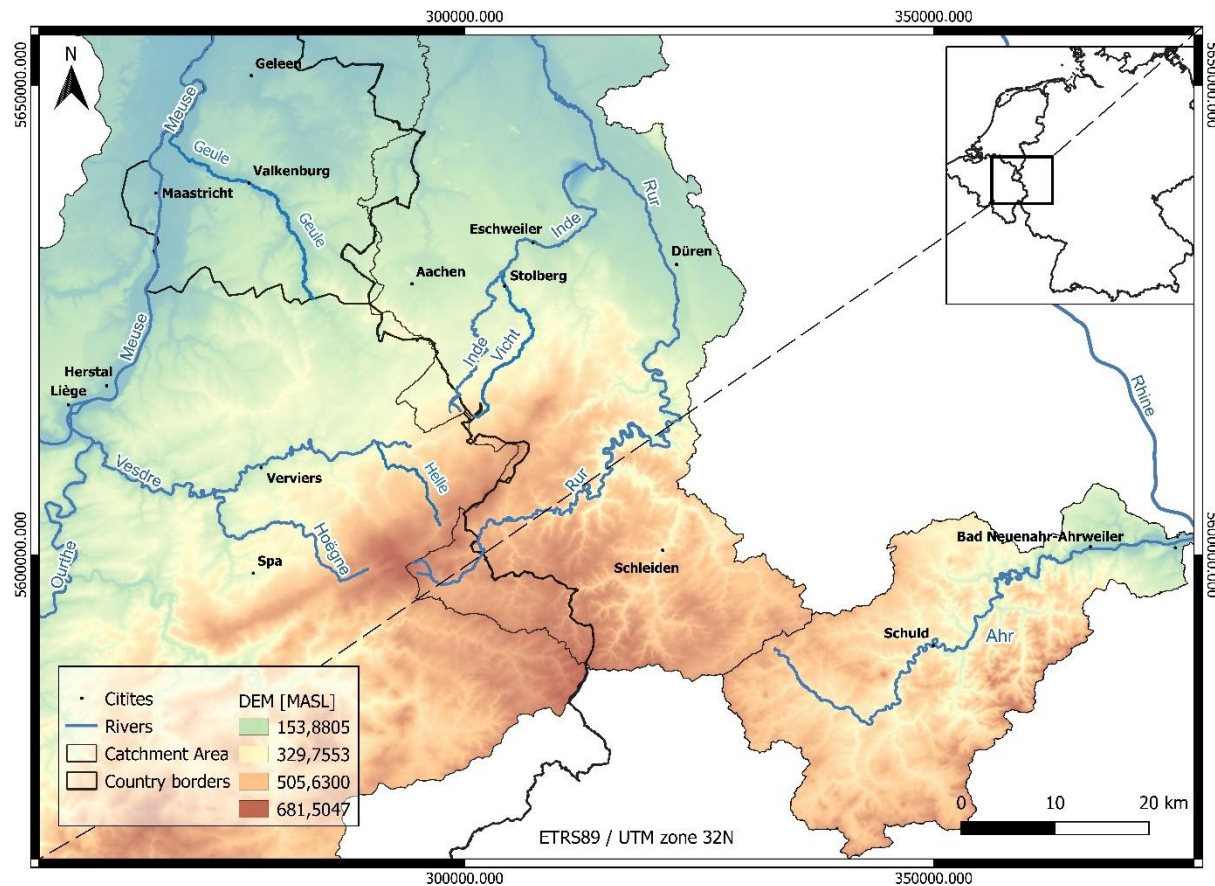


Figure 2: The study Area in Germany, Belgium and the Netherlands

1.2 Objectives

This study aims to better understand the processes and consequences of floating debris accumulation at bridges during a flood event. This study is part of the EMfloodResilience research project on flood risk and preparedness. Specifically, it reports the results of Work Package 4.1.1, on the data collection, modelling and prediction of floating debris accumulation. The work package has been divided in three successive steps (Figure 3). First, the characteristics of floating debris accumulations and the structures clogged by debris are analysed and documented in a database. Based on typical conditions observed, experiments are conducted with different debris compositions, hydraulic conditions, and bridge designs in order to quantify the backwater rise induced by clogging. For future reference, all experimental results are published in a second database. With the help of the field observations and experiments, recommendations for the design of bridges as well as and the operational procedures are established. The work has been performed in close collaboration by research teams at RWTH Aachen (Germany), TUDelft (The Netherlands) and ULiège (Belgium).

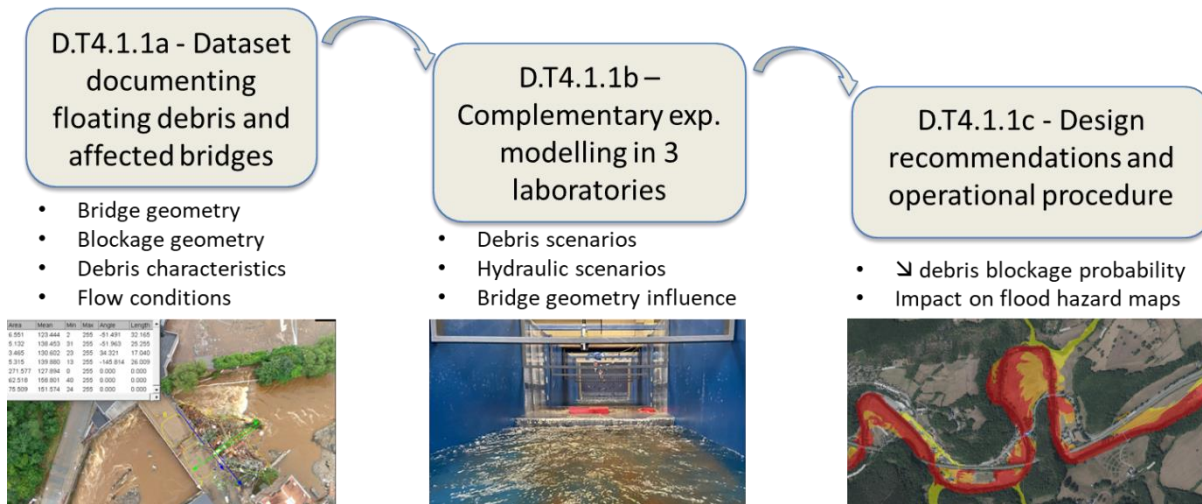


Figure 3: Structure of the work package depicted in this report

1.3 Report outline

In chapter 2, field data of debris accumulations at river structures during the 2021 flood event is collected and analysed. This data is also published in a database, which acts as a basis for the experimental modelling of debris accumulations described in chapter 3. Chapter 3 first explains the test setups as well as debris and bridge characteristics applied in the experimental modelling. Next, the results and conclusions from the experiments are summarized. The full results of the experiments are available online in a database. Chapter 4 states the recommendations for the design of bridges as well as operational procedures, drawn from the collected field data and experimental modelling.

1.4 Content

This report has the following content:

- A description of the database (field data) that is uploaded on the project website, in chapter 2, starting from page 14
- A synthesis of the field data in chapter 2.2, starting from page 15
- A synthesis of the experimental modelling and its outcomes in chapter 3, starting from page 19
- A description of design recommendation in chapter 4.1, starting from page 34
- A description of operational procedures in chapter 4.2, starting from page 35

Additionally, the dataset of the experimental results is uploaded on the project website.

2 Field data: debris accumulation during the 2021 floods

2.1 Field data: collection methods and database description

In total, 71 bridges affected by debris clogging are documented in a database and studied: 38 in Belgium and 33 in Germany, mainly at the rivers Vesdre and Ahr, respectively. In addition, one culvert in the Netherlands is studied, along the river Geul. Debris accumulation data is mostly based on aerial and handheld photos of the accumulations: field surveys arrived late for in-situ investigation of debris, since accumulations had often been removed quickly after the flood to restore discharge capacity. The database and analysis focus on three main aspects of debris accumulation:

- (1) Properties of the structure: location, damage and geometry, including the general bridge design and properties of pier, deck and railing.
- (2) Local hydraulic conditions, including estimated peak water levels, discharges, and, for the Ahr, widths of the inundated areas (river widths) during the 2021 flood.
- (3) Accumulation properties, including estimated accumulation dimensions (maximum width, length and height, estimated volume), its position at the structure, and the debris composition.

Structure properties are based, in preferential order, on 1) Construction drawings; 2) Georeferenced maps and orthophotos from an online cartographic portal; 3) In situ measurements or 4) Post-event pictures, where the first available source on the list was used. For the hydraulic conditions, peak water levels and discharges in Germany are based on reconstructed gauge data from the State Office Landesamt für Umwelt Rheinland-Pfalz in Germany (personal communication, 2022). The flow widths, supplied for the river Ahr, are based on surveying data conducted by Hydrotec and Ernst Basler+Partner for the Landesamt für Umwelt Rheinland-Pfalz in Germany and estimated coverage of the inundation areas by the same State office (personal communication, 2022). In Belgium, water levels are based on a post-event field survey performed by the Walloon Administration. Discharges are based on hydrological modelling of the flood event from distributed rain data performed by Liege University. Accumulation properties in the database are based on analysis of handheld and aerial photos taken during or directly after the flood. An overview of the parameters recorded and published in a database can be found in Appendix 1.

Photo analysis

The software ImageJ (Version 1.53) was used to measure lengths and surfaces from pictures, using data from the structure's geometry or surrounding structures to determine the scale. Information based on photos from different perspectives, including aerial and handheld photos, was combined here to obtain both horizontal and vertical dimensions. To maximize the accuracy of the estimations gained from pictures analysis, three cases were first analysed by three different researchers. After comparison of the results, variations between researchers were limited: for example, below 15% for accumulation volumes. For all following bridges, each evaluation was performed individually by two different researchers. If their estimations varied less than 15%, the average value was encoded in the database. If they varied by more than 15%, results were discussed to get a value approved by both researchers.

For each debris accumulation, the debris composition was described by the estimating volume fraction of several debris categories. These categories were: A) natural wood (trees), B) anthropogenic wood (construction wood, plates, beams), C) plastic tanks/containers; D) metal tanks/containers; E) vehicles (cars and caravans); F) household items (furniture etc.); G) industry items (large installations) and H) building rubble (not fully wooden, e.g. roof parts, insulation).

Based on these debris categories, the debris shapes present in each accumulation were analysed, as object shape likely governs their blocking probability, the degree of interlocking between debris pieces and the permeability of both individual debris pieces and the full accumulation. Hereto, the volume of debris in each of the debris categories is divided between elongated shapes (referred to as 'logs'), flat shapes ('plates') and bulky objects ('cubes'), following the ratios in Table 1. This results in an estimate of the fraction of log-shaped, plate-shaped and cuboid debris in every accumulation.

Table 1: The debris categories distinguished in the database, and the ratios used to translate this into volume fractions for log-shaped, plate-shaped and cuboid debris.

Debris type	Log fraction	Plate fraction	Cube Fraction
Natural wood	1	-	-
Anthropogenic wood	0.5	0.5	-
Tanks and containers	-	-	1
Vehicles	-	-	1
Household items	0.2	0.4	0.4
Industry items	0.2	0.4	0.4
Building rubble	0.5	0.5	-

2.2 Field data: results and synthesis

With the help of the data collection on debris accumulation, the total volumes as well as the different debris compositions were determined, and characteristic bridge designs established. The observed debris accumulations at the bridges in Belgium and Germany ranged in size from a few m³ to more than 4000 m³, i.e. up to 88 m³ per meter of bridge length. Especially large accumulations were able to disrupt the normal flow of the river and cause substantial backwater rise (Figure 4). Moreover, debris accumulation and flooding caused widespread bridge damage. Of the 71 bridges with debris accumulation, 13 were structurally severely damaged and a further 19 too damaged to be kept in service. In the Netherlands, no significant bridge clogging was identified. Clogging did occur at one submerged culvert, near Bunde. Although the accumulation was relatively limited compared to those in Belgium and Germany, the resulting reduction of the already insufficient culvert discharge capacity means the debris intensified local flooding.



Figure 4: Two extreme examples of debris accumulation, with trees, building rubble, caravans, tanks and other materials show the backwater rise caused by accumulations. Location: Kreuzberg, Germany and Pepinster, Belgium.

Looking at the debris accumulations and their composition, about 50 percent of the debris volume consisted of trees, the remainder of manmade materials: mostly building rubble, construction wood and, in Germany, vehicles (Figure 5). The manmade fraction is uncommonly high – previous research typically found accumulations largely consisting of trees (Diehl, 1997; Lucía et al., 2015; Rusyda et al., 2014; Steeb et al., 2017) – due to the many settlements built directly along the river in the study area, and to the studied bridges predominantly being located in exactly these urbanized areas.. Building rubble, (crushed) caravans and other manmade objects differ in shape and permeability from trees, allowing heterogeneous mixtures to form accumulations with a very low permeability and porosity. Consequently, these accumulations can cause substantially more backwater rise. This means existing relations that estimate the backwater rise of natural accumulations can lead to a dangerous underestimation of the flood risks in urban environments, when making flood hazard maps or evacuation decisions. Hence, more research on the effect of debris shape and type on backwater rise is urgently needed. A part of this research already takes place within this project (chapter 3), with flume experiments that study the effects of different debris shapes, based on the typical debris shape composition found in the debris database (Figure 5).

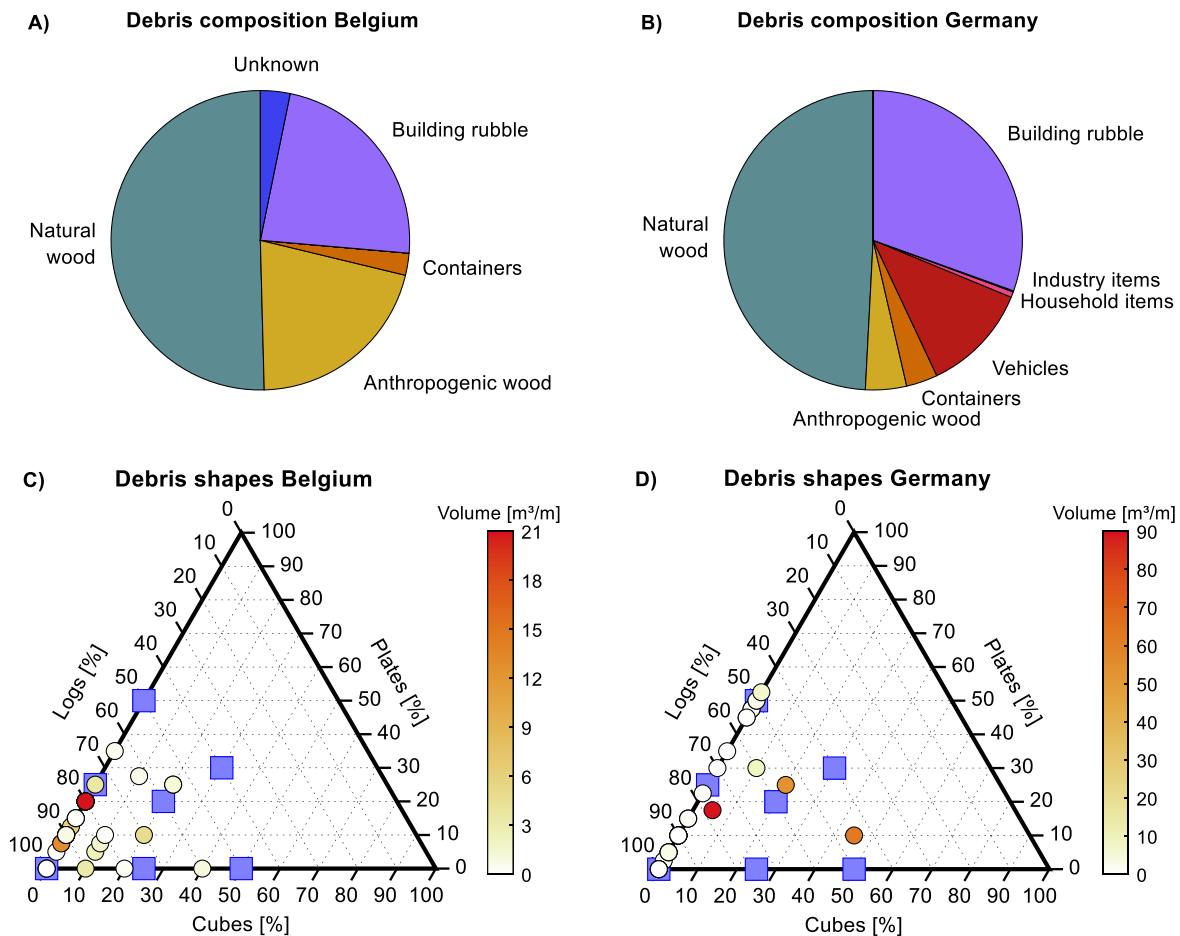


Figure 5: Debris compositions observed from the field data after the flood event 2021. Blue squares in subplot C) and D) indicate debris mixtures studied in the experiments (Chapter 3.1.4).

Next, the bridge design and geometry at all debris accumulations were studied. In both countries, the largest accumulations occurred at bridges where the distance between piers was small (≤ 10 m), allowing large blocked trees to bridge the distance between piers, thereby initiating clogging (Figure 6A, 6B). Simultaneously, at the majority of the bridges, and at all bridges with large accumulations, peak water levels reached at least the bridge deck, and frequently exceeded it by several meters (Figure 6C, 6D). This has major implications: first, having water reaching the superstructure (deck and railings) means that the deck and railing will already be responsible for backwater rise, irrespective of any debris. Secondly, it means the superstructure interacts with debris, with debris being blocked by the deck and railing, or, if the water level is high enough, flowing over the bridge to continue downstream. Third, this results in additional forces on the bridge superstructure, such as buoyancy forces, which can endanger the stability of the bridge.

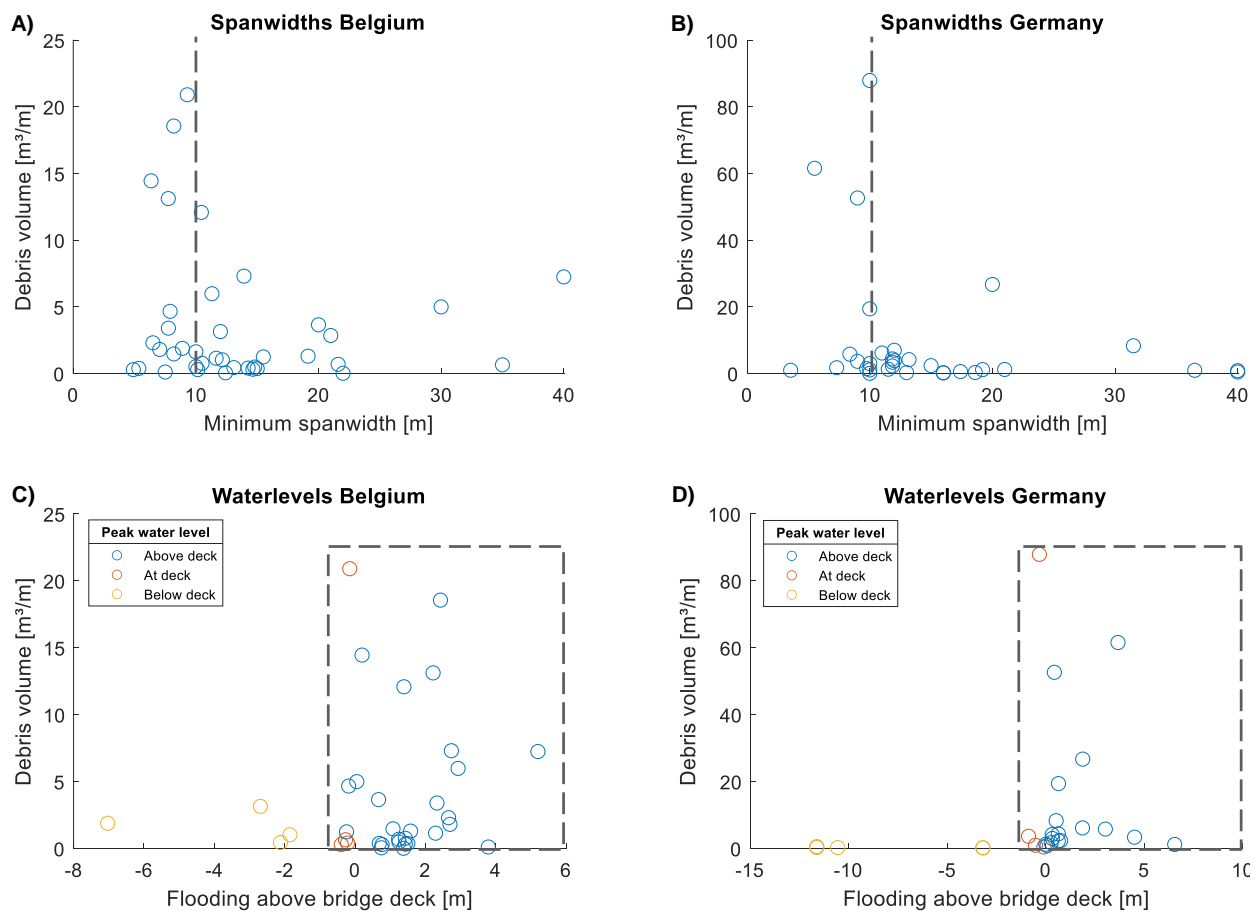


Figure 6: Observed debris volumes, per unit meter width as a factor of span width (pier spacing) and flood height above the river deck. Dashed lines indicate the region where large accumulations are most likely.

Looking at the bridges with the largest accumulations in Belgium and Germany, as these are most interesting to study in more detail, the mean opening width was 8.5 m and at least two piers were present, with a mean pier width of 1.1 m. The opening height (between bridge deck and river bed) was on average 4.3 m and the bridge width, measured in the flow direction, 8 m. A mean handrail height of 1 m was found.

Overall, the collected information on debris composition and bridge design helps to better understand the bridge clogging process. In addition, the collected data will be used in chapter 3 to define the design of the bridge used in flume experiments, as well as the various debris mixtures.

3 Experimental modelling

3.1 Experimental methods and database description

Experiments were conducted to quantify the backwater rise caused by debris accumulations, and how this depends on debris composition, hydraulic conditions and bridge design. These experiments were conducted in three laboratories in Liège, Aachen and Delft, in order to efficiently conduct a large number of experiments. The experimental setup and test scenarios were chosen based on typical conditions and bridge designs from the debris accumulation database (see chapter 2.2). Within section 3.1, the laboratory characteristics of all three laboratories will be described, as well as the test method and scenarios. Experimental results will be discussed in section 3.2.

The experimental modelling was divided into three phases: the variation of the debris composition, the flow conditions and the bridge design (see Figure 7). In total 285 experiments were conducted for this part of the deliverable. To maximize comparability between labs, the test setups at all three labs were as similar as possible. In all three labs, tests at 1:16 scale were performed in flumes of 1.2 m width. In Liège, tests were additionally performed at a 1:18 scale in a flume of 1 m wide. A bridge was present in each of the flumes, all with the same height for the 1.2 m wide flumes. Debris was dropped into the flume, every three minutes in small batches from a drop-in device, to measure how backwater rise increases with debris volume. Any debris that passed the bridge was immediately re-added with the drop-in device, to ensure the accumulation volume at the bridge equals the known dropped-in volume. For the debris composition tests, the effect of seven different debris mixtures (based on the mixtures determined in chapter 2) on clogging and backwater rise was studied, under fixed hydraulic conditions and bridge design (see chapter 3.1.2). For the second experimental phase on flow conditions, the initial water depth and the Froude number were varied. For the analysis of the bridge design, the opening shape, the number of piers and the handrail design were varied. During these tests, the water levels were recorded by ultrasonic water level sensors upstream and downstream of the bridge. The test setups in all three labs, debris mixture and test program are described in more detail below.

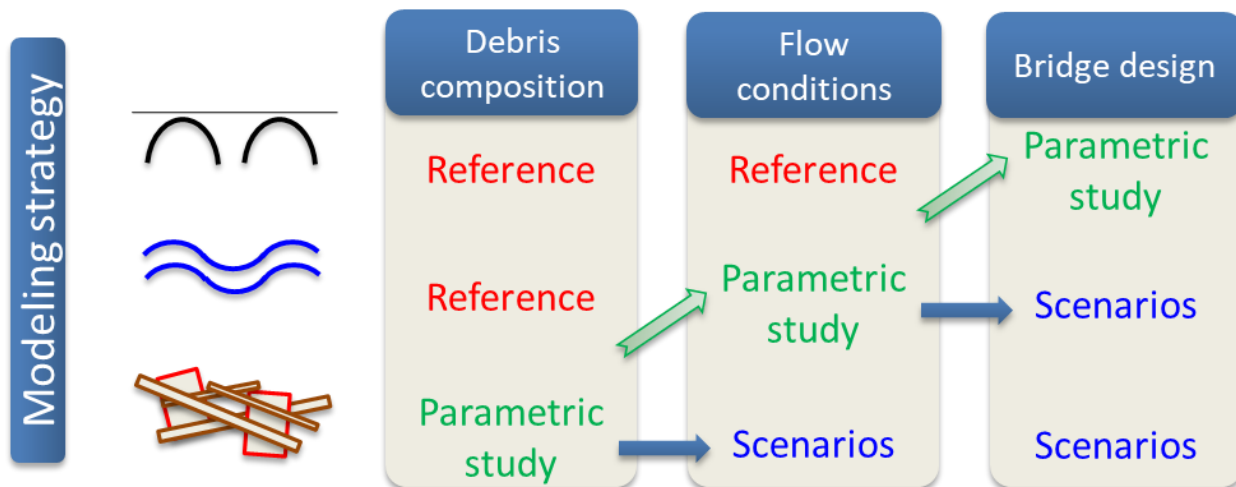


Figure 7: Modelling Strategy

3.1.1 Test setup: labs and flumes

Flumes Liège

In Liège, the experiments were conducted in two flumes in order to investigate several bridge designs. The metal flume with a width of 1.2 meters is further referred to as flume B1 (for Belgium 1). This is the same flume width as used in the other labs. Over a length of seven meters, it has no inclination. Five ultrasonic distance sensors are placed along the channel to record the changes in water levels. The first sensor is placed four meters upstream of the downstream edge of the bridge. Two more sensors are placed 2.5 and 1.5 meters upstream of this edge. The fourth sensor is placed centrally above the bridge and one sensor records the water level variations one meter downstream of the downstream edge of the bridge. The drop-in device is located three meters upstream of the bridge at a height of 0.8 meters from channel bottom. A metal grid and a synthetic screen are used at the inflow of the channel for flow straightening. A downstream weir allows the adjustment of the hydraulic conditions while the debris is stopped by a horizontal mesh at the end of the channel. A maximal discharge of $0,24 \text{ m}^3/\text{s}$ can be achieved.

The second flume (shown in Figure 8) is composed of a glass bottom with a width of one meter and a height of 0.5 meters and is further referred to as flume B2. Over a length of 10 meters, it also shows no inclination. Again, five ultrasonic water level sensors (UDS) are placed along the channel (Figure 8). The drop-in device is located five meters upstream of the bridge at a height of 0.5 meters from the channel bottom. The inflow enters through a metal grid and a synthetic screen while a weir is used at the end of the channel. A peak discharge of $0.1 \text{ m}^3/\text{s}$ can be achieved within this flume. The bridge design is adapted to the narrow width of one meter compared to the other flumes and will be further described in chapter 3.4.2.

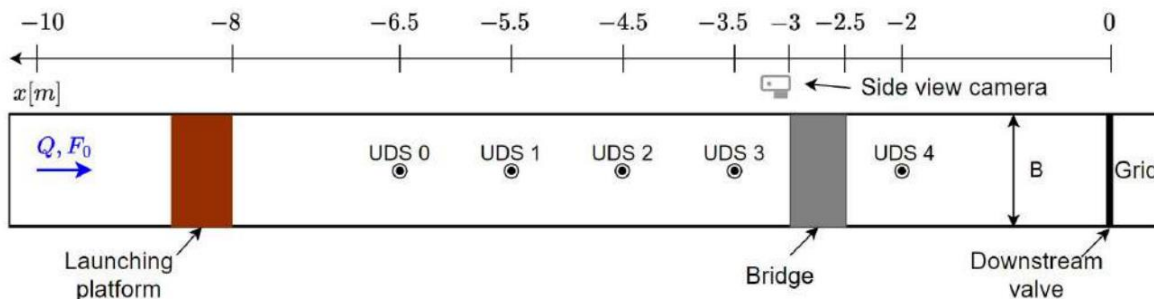


Figure 8: Experimental set-up for the flume B2 in Liège

Flume Aachen

The experiments in Aachen were conducted in a 32-meter long and 1.7-meter-wide concrete flume as shown in Figure 9 which is further referred to as flume G1. To narrow the flume to the width of 1.2 meters used in all three labs, two masonry walls with a height of 0.75 meters were built over a length of 10 meters. After the inlet reservoir with a length of four meters, the water passes a flow equalizer that reduces turbulence. Two metal plates form the inlet for the main experimental area and the 1.2-meter-wide flume. A drop-in device was constructed in order to reduce the two-meter height difference for the insertion of debris and the creation of waves. Between the drop-in device and the bridge, four ultrasonic water level sensors are placed every meter. One water level sensor is placed centrally above the bridge and another

sensor one meter downstream of the center of the bridge. Finally, the outflow is located approximately five meters downstream of the bridge. A vertical mesh is placed on top of the drain opening in order to collect debris which passes the bridge. Two cameras are located centrally at the bridge, one on top of the bridge facing towards the drop-in device, another one outside of the flume behind a glass wall. With the help of four pumps, a maximal discharge of $1.2 \text{ m}^3/\text{s}$ can be created within the flume. The flume has no inclination. With the help of an ADV (Acoustic Doppler Velocimeter) the flow velocity within the channel is measured once for every hydraulic condition, that is tested within the different scenarios. A velocity profile is recorded 4.5 meters upstream of the bridge.

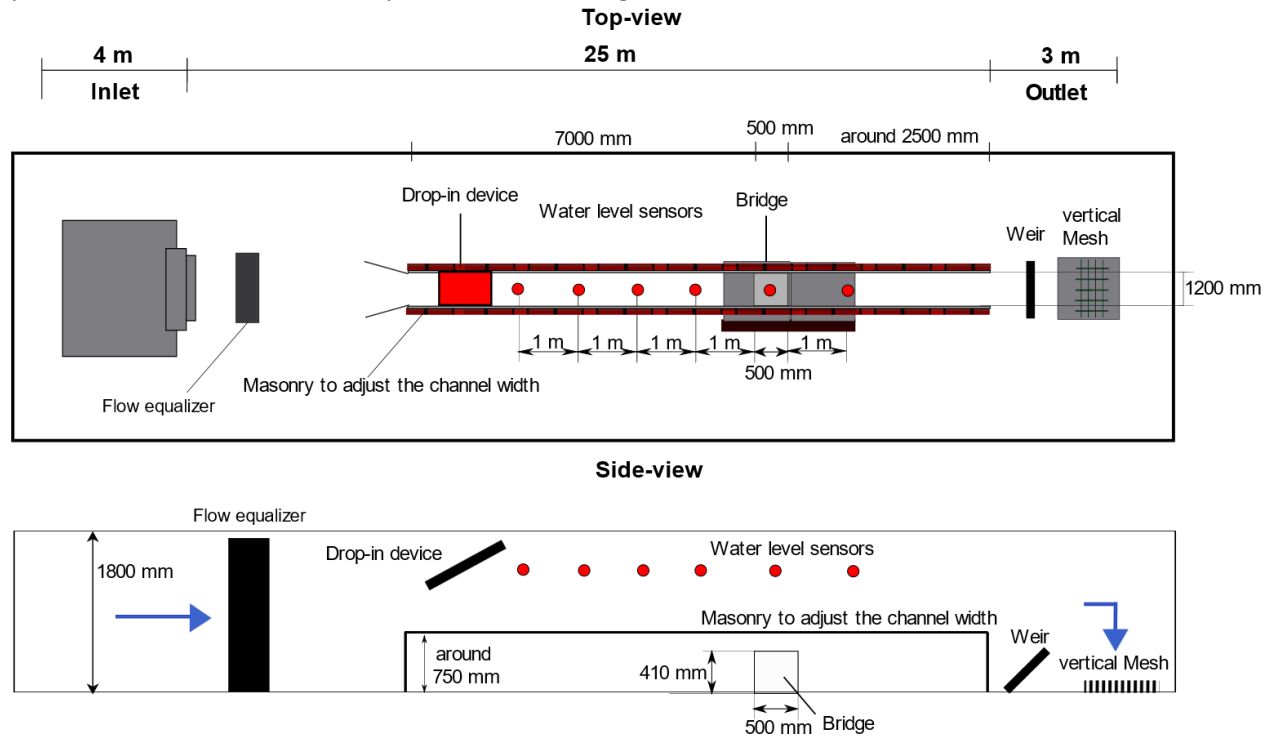


Figure 9: Experimental set-up in the flume G1 in Aachen

Flume Delft

This 40-meters-long outdoor flume, referred to as flume N1, is characterized by two different sections. Measurements take place in the first 14 meters, which have been narrowed to 1.2 meters for comparison with the other labs (Figure 10). The channel is 1.5 m deep, with a flat bottom. Five ultrasonic water level sensors are placed in the channel. Four of them are placed at 6.5 meters, 3.5 meters, 1.5 meters and 0.25 meters upstream of the downstream edge of the bridge. The last sensor is placed one meter downstream of this edge. A top view video camera (GoPro Hero10) is located at a height of two meters above the channel bed and 1.5 meters upstream of the downstream edge of the bridge. The inflow of the channel is characterized by an inclined plate with longitudinal flow straighteners. At the outflow, the water depth is regulated by a weir to limit backwater effects and to regulate the downstream water level. Its position was varied during the experiments from 29 meters downstream of the bridge to 20 meters. A horizontal rack is used to stop the debris at the outflow. The drop-in device is located five meters upstream of the bridge at a height of 0.8 meters. A maximum discharge of $0.10 \text{ m}^3/\text{s}$ can be reached in this flume.

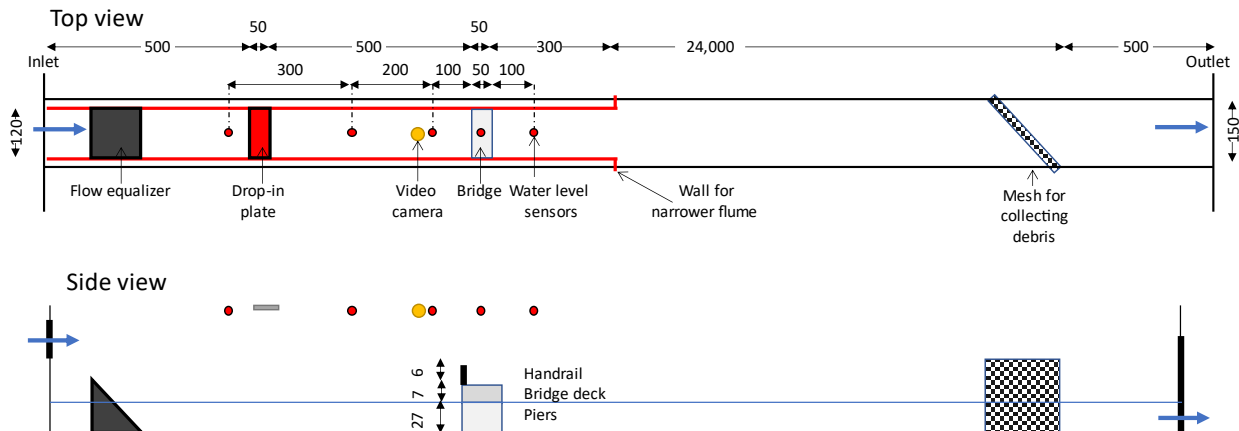


Figure 10: Experimental setup in Delft

3.1.2 Test setup: bridges

With the help of the typical bridge characteristics determined in chapter 2.2, the model scale was determined for the flumes. Since a bridge with two piers and two openings should be represented, the total width of the bridge resulted in $8.5 \text{ m} \times 2 + 1.1 \text{ m} = 19.2 \text{ m}$. In the 1.2 m wide flumes in Delft, Aachen and the flume B1 in Liège this resulted in a model scale of 1:16. The model scale for the second flume in Liège B2 with a width of 0.985 m was 1:18. Applying these model scales, the bridge dimensions displayed in Figure 11 and Figure 12 were determined. In all labs, bridges for the 1:16 scale, were 1.2 m wide, with two piers and a freeboard of 27 cm between the deck and bed. In Delft and Liège, bridges openings were rectangular, in Aachen an arched bridge with radius of 35.5 cm for the arch was constructed due to the high share of arch bridges within the database for German bridges. The bridges were also exchanged between Aachen and Liège to further analyze the effect of the opening shape. The handrail was made of 2 mm thick steel bars with a length of 6.5 cm and 10 mm spacing in-between resulting in a porosity of 77%. A horizontal bar with the thickness of 5 mm was added on top of the bars. In the 1:18 flume in Liège (flume B2), a bridge with either one or two piers was tested, without handrail.

To determine the effect of bridge design, various adaptations to the standard design described above were tested. The influence of the number of piers was investigated using bridges with one or no piers. In Aachen and in Delft, the handrails design was also varied. In addition to the porous handrail described above, tests were conducted without handrail, with a closed handrail (wall) and with a closed handrail plus streamlined, rounded deck. In Delft, a lower version of the bridge with rectangular openings was tested, with the bridge deck at 20 cm instead of 27 cm.

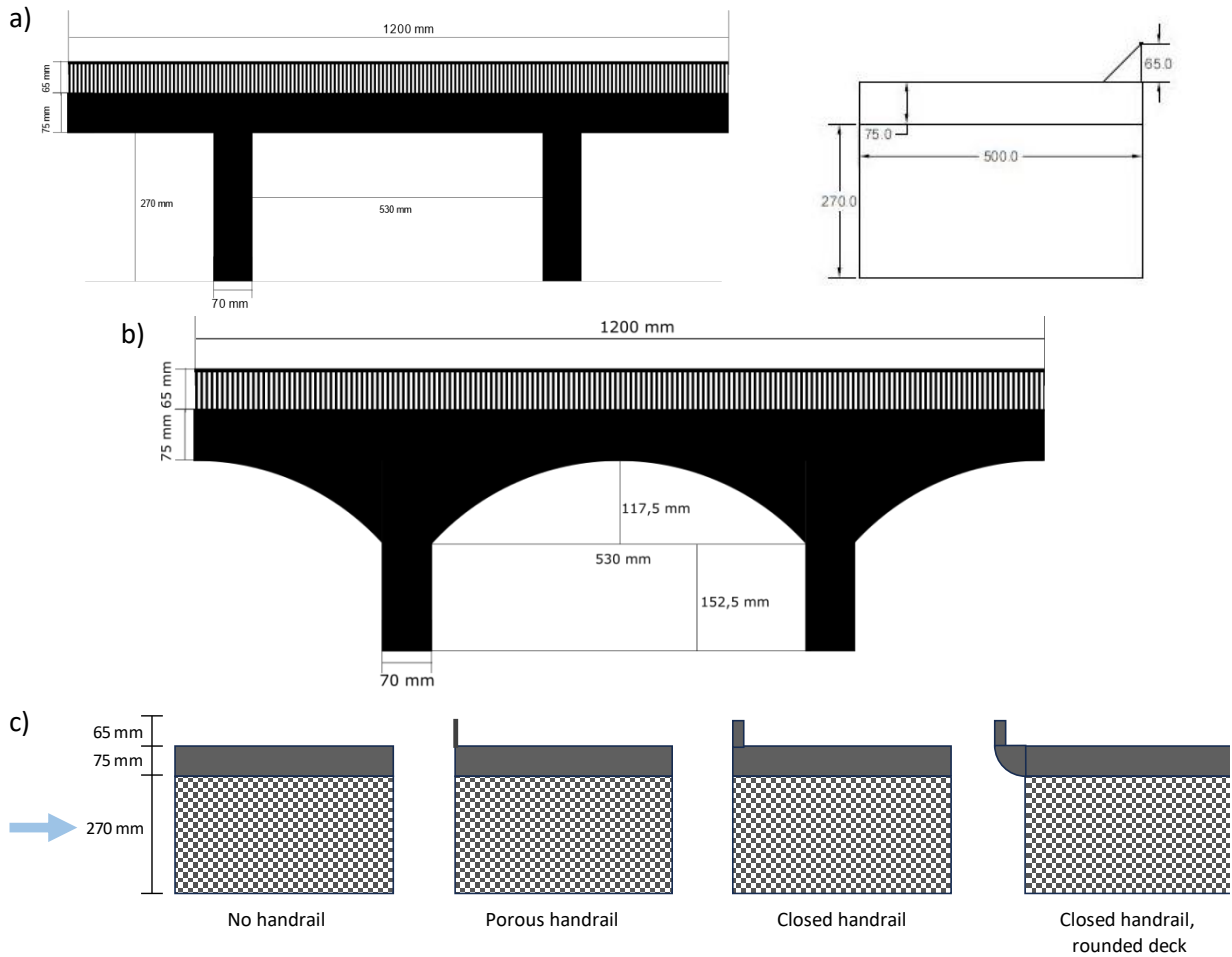


Figure 11: Bridge dimensions for the model scale 1:16. a) Rectangular bridge opening, b) arched opening and c) sideview of the different handrail designs

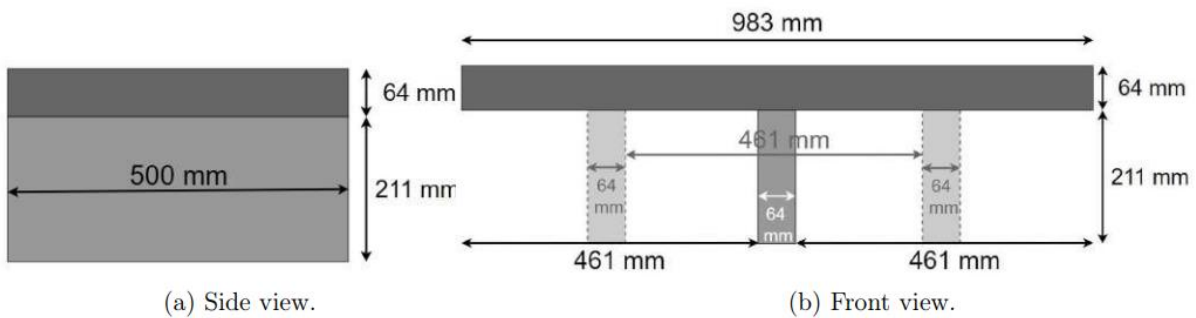


Figure 12: Bridge dimensions for the model scale 1:18 with no handrail and the two pier variations

3.1.3 Test setup: debris

Three types of debris were considered in this study: logs, cubes and plates. Logs were represented by sticks with a length of 10 cm up to 80 cm. Flat objects such as building rubble or panels from destroyed caravans were imitated by blue plywood plates with a thickness of 2 mm, a height of 60 mm and a length of 100 mm. Voluminous objects like cars and tanks were represented by red wooden cubes from Douglas fir with the size 9 × 9 × 18 cm. Based on debris compositions of accumulations during the 2021 flood event (chapter 2), seven different debris mixtures were created, shown in Table 2. In Appendix 2, the detailed compositions with the corresponding number of logs, plates and cubes for each debris composition is listed. Furthermore, weight and density measurements for the debris components in wet and dry stage can be found in Appendix 3.

During experiments, a small batch of debris was dropped into the flume every three minutes, to measure the backwater rise as a function of debris volume. For the debris composition tests, a debris volume of 190 liters was used, tested at the 1:16 scale flumes in Liège and Aachen. This volume was defined based on the characteristic large wood volume proposed by Schalko (2018). Depending on the tested debris mixture, individual debris batches were between 4.5 liters and 9 liters, giving a maximum of 40 debris batches dropped in the flume during a test. For the tests on flow conditions and bridge design, a debris volume of 76 liters was used for the model scale of 1:16 and a debris volume of 50 liters for the model scale of 1:18 in Liège. For these tests, the mixtures with 75% logs and either 25% plates or 25% cubes were used.



Figure 13: Debris components

Table 2: Modelling scenarios with different debris compositions

Debris Composition	Used for tests on		
	debris composition	hydraulic conditions	bridge design
100% Logs	✓		
75% Logs, 25% Cubes	✓	✓	✓
75% Logs, 25% Plates	✓	✓	✓
50% Logs, 50% Cubes	✓		
50% Logs, 50% Plates	✓		
60% Logs, 20% Plates, 20% Cubes	✓		
40% Logs, 30% Plates, 30% Cubes	✓		

3.1.4 Test program

As described above, tests were conducted in three phases, for the effect of debris composition, hydraulic conditions and bridge design. A full list of all 285 tests can be found in Appendix 4. A summary of the test program is given below.

Debris composition

Debris composition tests were conducted at an initial Froude number of 0.28 and an initial water depth of 27 cm, right at the underside of the bridge deck. The default bridge with two piers and a porous handrail was used. The tests with different debris compositions (Table 2) were repeated three times in both Aachen and Liege (flume B1).

Hydraulic conditions

Tests for the effect of hydraulic conditions were conducted in all three laboratories. For these tests, the initial water level varied between 10 cm and 39 cm. The Froude number was varied between 0.13 and 0.6. This Froude number is a dimensionless number that describes the ratio between inertia and gravity forces. It is expressed by the ratio of the flow velocity v and the wave propagation velocity in open channels (i.e. $(gh)^{0.5}$, with g the gravitational constant and h the flow depth): $Fr = \frac{v}{\sqrt{gh}}$. For these experiments, only the debris compositions containing 75% of logs and 25% of plates or 25% of cubes were used since these were the most representative and had clearly different effects on backwater rise. The tests were usually repeated at least two times to enhance result robustness. Details can be found in Table 3, Table 4 and Figure 14.

Table 3 : The hydraulic conditions and number of repetitions for the experiments conducted at 1 :16 scale in Delft, Liege and Aachen, using a porous handrail and two piers. #/# refers to the number of repetitions with 25% plates resp. 25% cubes and 75% logs, h_0 is the initial water level and Fr_0 the initial Froude number at the beginning of each experiment

Bridge design	Fr_0	h_0 [cm]							
		15	22	24	27	30	33	35	39
Rectangular	0.13				2/1				
	0.2								
	0.27-0.28	2/2	2/1		4/3	2/2		4/4	
	0.4	2/2	2/2		2/2	3/4		2/2	
Arched	0.5	2/2	2/2		2/2				
	0.13		3/1		4/4		1/2		
	0.21		0/1	2/0					
	0.27-0.28		0/1		7/7				2/0
	0.4				2/0				

Table 4: The hydraulic conditions and number of repetitions for the conducted experiments at 1 :18 scale in Liège, using two piers, no handrail and rectangular openings. #/# refers to the number of repetitions with 75% logs and 25% plates resp. cubes, h_0 is the initial water level and Fr_0 the initial Froude number at the start of each experiment

Fr_0	h_0 [cm]						
	10	15	20	21	24	31	37
0.13				4/4			
0.2						(1/1)	
0.27	2/4	2/2	2/2	2/2	2/2	2/1	
0.4	2/2	2/2	2/2		2/2		
0.6	2/2	2/2	2/2				

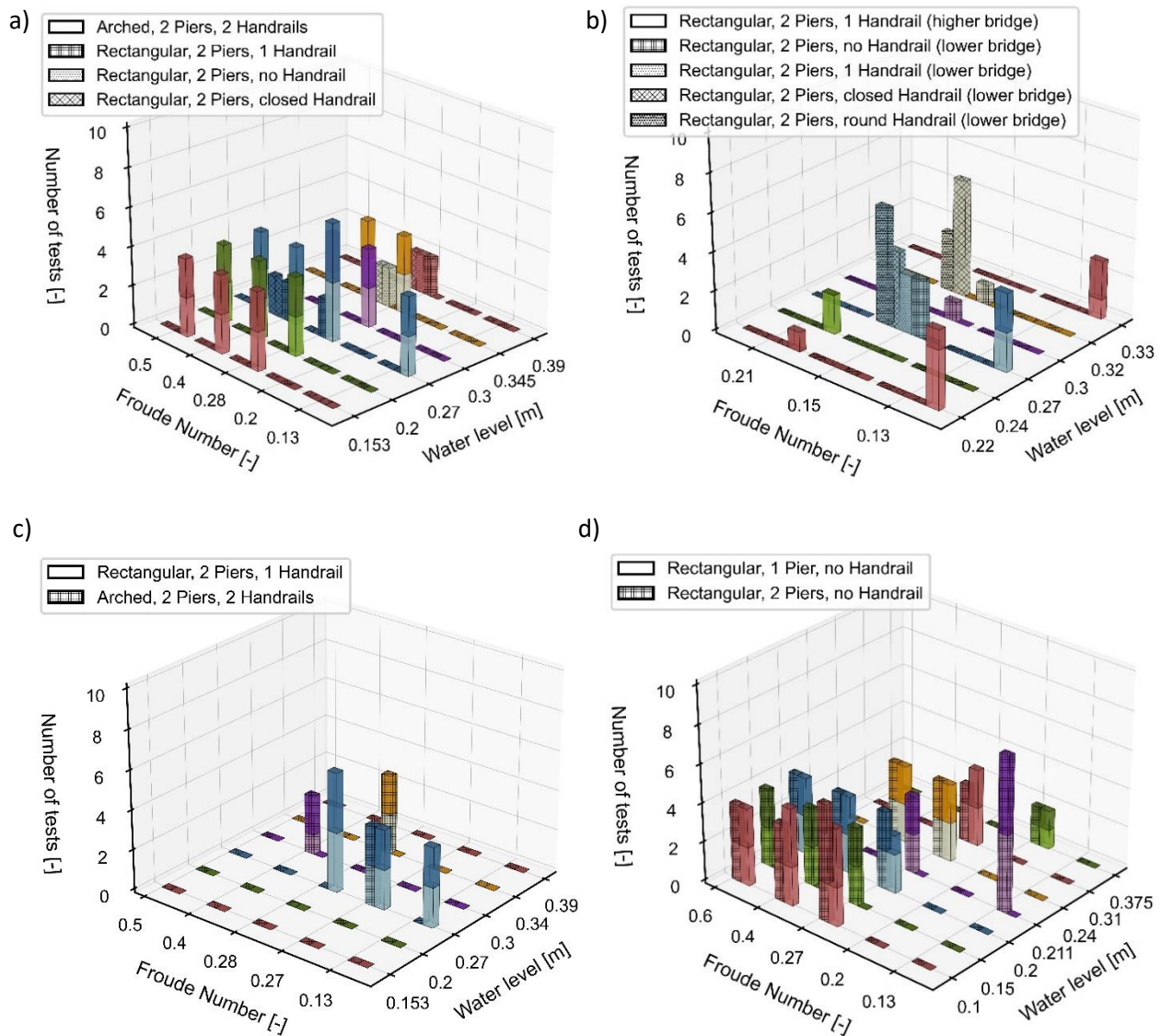


Figure 14: Overview over the different bridge designs tested with debris compositions containing 75% of logs and 25% of plates (lower bar) and 25% of cubes (upper bar) in the labs in Aachen (a), Delft (b), Liège flume B1 (c) and Liège flume B2 (d). Different colours indicate different initial water depths, fill patterns bridge designs.

Bridge Designs

Tests on the effect of different bridge designs were conducted in all three labs. In Liege, tests were conducted with one pier instead of two in flume B2. In Delft and Aachen, tests were conducted on the effect of the railing, using setups with A) the default porous handrail, B) no handrail, C) a closed handrail (wall), and D) a closed handrail in combination with a streamlined, rounded deck. All these tests were performed using a bridge with rectangular openings. In case of Delft, the bridge was lowered by 7 cm, giving a freeboard of 20 cm. In addition, the bridges with arched and rectangular openings were exchanged between Aachen and Liège to further analyze the effect of the opening shape. Details of the conducted tests can be found in Table 5, Table 6 and Figure 14

Table 5: The hydraulic conditions and number of repetitions for the alternative bridge designs tested at 1:16 scale in Aachen and Delft, all with two piers. #/# refers to the number of repetitions with 25% plates resp. 25% cubes and 75% logs.

Bridge	Handrail	Fr _o	h _o [cm]					
			27	30	32	35	39	
high	0 HR	0.28					2/0	
bridge	Wall	0.28					2/0	2/0
low	0 HR	0.15	3/0	1/0	1/0			
bridge	1 HR	0.15	3/0		3/0			
	Wall	0.15	4/0		6/0			
	Wall, rounded	0.15	6/0		3/0			

Table 6 : The hydraulic conditions and number of repetitions for the bridge with one pier tested at 1 :18 scale in Liège (flume B2), without handrail. #/# refers to the number of repetitions with 25% plates resp. 25% cubes and 75% logs

Fr _o	h _o [cm]				
	10	20	24	31	37.5
0.2					1/1
0.27	2/3	2/1	2/2	2/2	
0.4	2/3	2/2	2/2		
0.6	2/2	2/2			

3.1.5 Database description and encoding

The results of the experiments were summarized in a database. For every test, the database first describes the test setup and conditions, in total giving an overview of the experimental program. Next, the results of each test are summarized, i.e. the water levels during the experiments as a function of the added debris volume. Appendix 4 gives an overview of all conducted tests, using the same names for tests as used in the database. These test names are based on the test conditions, consisting of the following aspects:

- Flume (G1, B1, B2, N1)
- Bridge opening shape (A for arched, R for rectangular)
- Number of piers (0P, 1P, 2P)
- Initial Froude number (F015, ...)
- Initial water depth [cm] (h32, ...)
- Debris composition (plates, cubes, logs, notes)
- Handrail (0HR for no handrail, 1HR/2HR for porous handrails, 1W for wall, 0 HR, 1RW for wall plus rounded deck)
- Other info, in filename
- Repetition (R1, R2, ...)
- Debris volume (76 L, 190 L)

Overall, this leads to a test name such as 'B1_R_2P_F028_h27_25C_75L_1HR_R1_190L'. In addition, a few test conditions not included in the test name are described in the database:

- Date of test
- Length of the debris carpet [m]
- Height of the debris carpet after the experiment, directly in front of the bridge [cm]
- Other remarks, e.g. on data quality

Next, the database summarizes the results of the tests, i.e. the evolution of water levels as more and more debris is dropped into the flume. For every debris batch added to the flume (between 5 and 40 batches per test, added three minutes after each other), the total debris volume is noted, as well as the water level at each of the UDS sensors. These water levels are moving averages over a one-minute period, to filter out short-term fluctuations.

3.2 Results of experiments and synthesis

3.2.1 Debris composition

As expected, results showed that the accumulation of debris at bridges induces significant backwater rise (Δh). This is consistent with observations during the flood. For this phase, only the debris composition was varied between tests, while the flow conditions ($Fr_0 = 0.28$ and initial water depth just below deck level) were kept constant. By varying the debris composition, it was observed that the backwater rise increased for debris compositions containing plates (see Figure 15 and Figure 16). Due to the presence of plates, debris accumulations became denser and less porous. The debris compositions containing 50% plates and 50% logs resulted in 150% more backwater rise than with solely logs for the tests conducted in Liège. In the other flumes a similar effect associated with the presence of plates could be observed, even though the extent of backwater rise varied slightly between the laboratories. The backwater rise with debris compositions containing cubes resulted in less dense debris accumulations and therefore lower backwater rise compared to compositions with 100% logs. Considering the model scale, backwater rise up to 4 m from the results in Liège and 1.6 m for Aachen can be determined when 25% of plates are included in the debris composition. The extent of backwater rise due to clogging at bridges during the 2021 floods has not yet been officially determined, however experts estimate the backwater rise at bridges with clogging at 2 – 3 meters (LfU, 2022). For the formation of a debris accumulation, a log that exceeds the pier distance was always necessary.

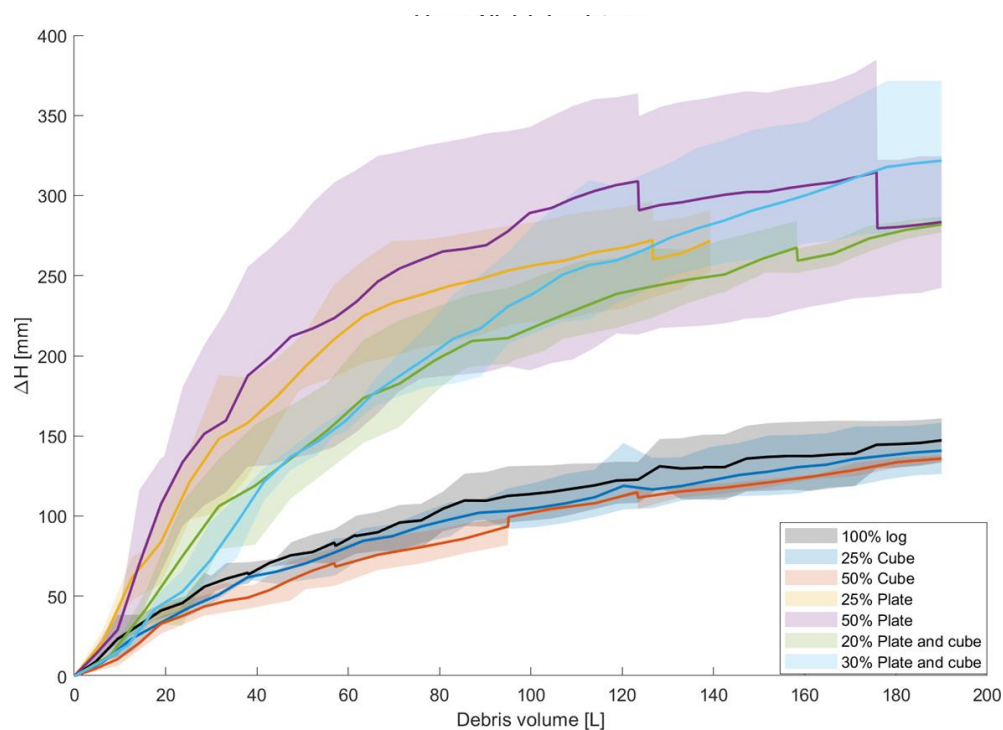


Figure 15: Backwater rise for the tests conducted with varying debris compositions in Liège. The initial water depth is 270 mm at a Froude number of 0.28, so e.g. $\Delta H=270$ mm signifies debris doubling the original water depth.

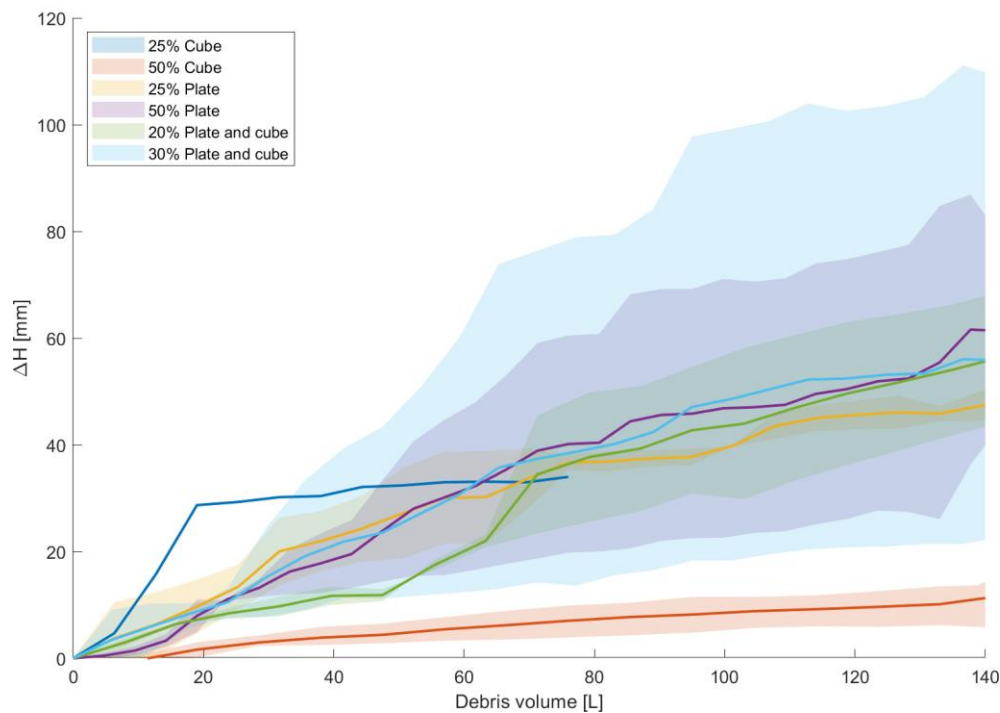


Figure 16: Backwater rise for the tests conducted with varying debris compositions in Aachen

3.2.2 Hydraulic conditions and bridge design

Numerical simulations of the flood event in 2021 at the river Ahr by the University in Aachen resulted in Froude numbers between 0.20 and 0.75 in front of the studied bridges. This range of Froude numbers was mostly covered by the laboratory tests. The variation of the hydraulic conditions showed that the relative backwater rise increases with an increasing Froude number (see Figure 17). Additionally, the relative backwater rise ($\Delta h/h_0$) decreased with increasing initial water depth (see Figure 18). The relation between relative backwater rise and Froude number does not seem linear and strongly depends on the height of the bridge deck. Furthermore, higher Froude numbers and a lower number of piers decreases the probability of clogging.

During the tests with different **handrails**, tests in Aachen showed that having a closed handrail (wall) increases the backwater rise by debris, compared to a porous handrail or no handrail (Figure 19). Similar tests in Delft, with the water level near (what would be) the top of the handrail, first showed that without handrail no debris is blocked, as all debris flows over the bridge. Secondly, having no handrail decreases the backwater rise caused by the bridge itself. A porous handrail adds some backwater rise and a closed handrail adds clearly more backwater rise by blocking the flow, while streamlining the bridge by rounding the deck decreases backwater rise (Figure 20, blue bars). Regarding backwater rise by debris (Figure 19, orange bar), backwater rise by the closed handrail is clearly larger, similarly to Aachen. In practice, having no handrail would not be safe, so this bridge design can be regarded as either a handrail that is already destroyed by floating debris, or as a handrail that can collapse when the bridge is flooded.

Between all three laboratories, a similar relation between the backwater rise und Froude number could be observed (slope of the lines in Figure 17). By exchanging the bridges between Aachen and Liège, it could

be observed, that the shape of the bridge opening shows only minor variations in the backwater rise (see Figure 21). The effect on the backwater rise further decreases with increasing Froude number. Furthermore, it could be observed, that the probability of clogging decreased as soon as the Froude number increased. Regarding tests with different **pier** configurations, it could be seen, that the probability of clogging reduced strongly when decreasing the number of piers.

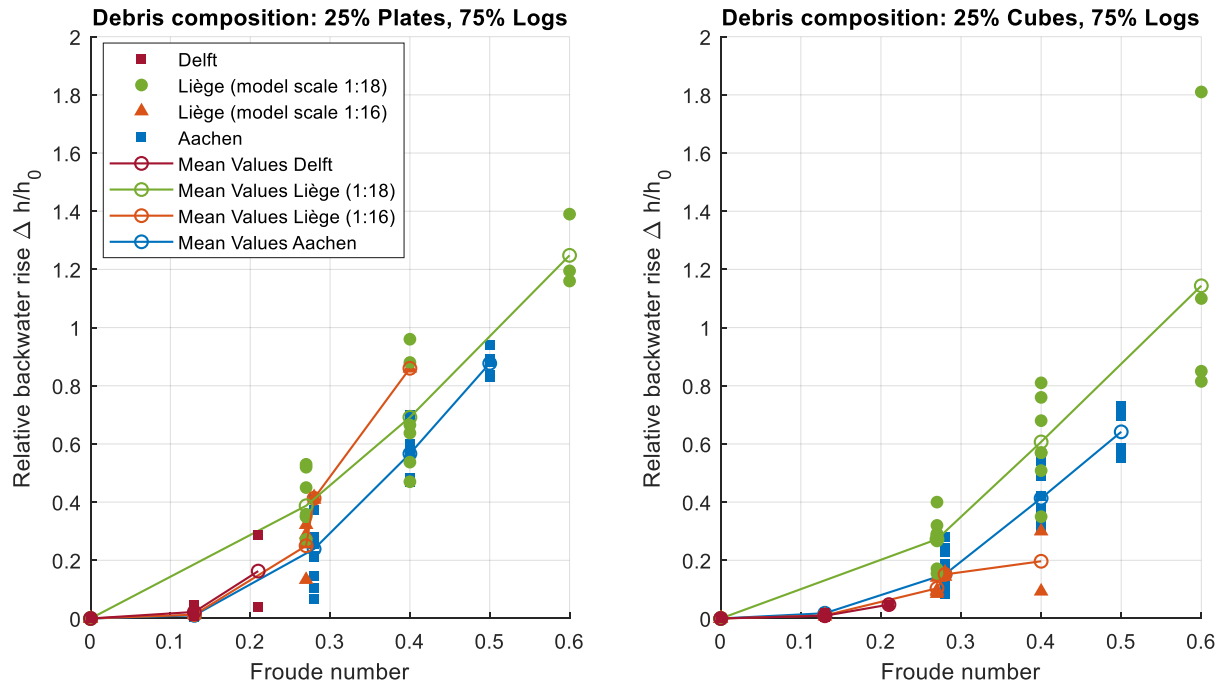


Figure 17: Relative backwater rise for the experiments conducted with a debris composition of 25% plates and 75% logs and 25% cubes and 75% logs for varying Froude numbers

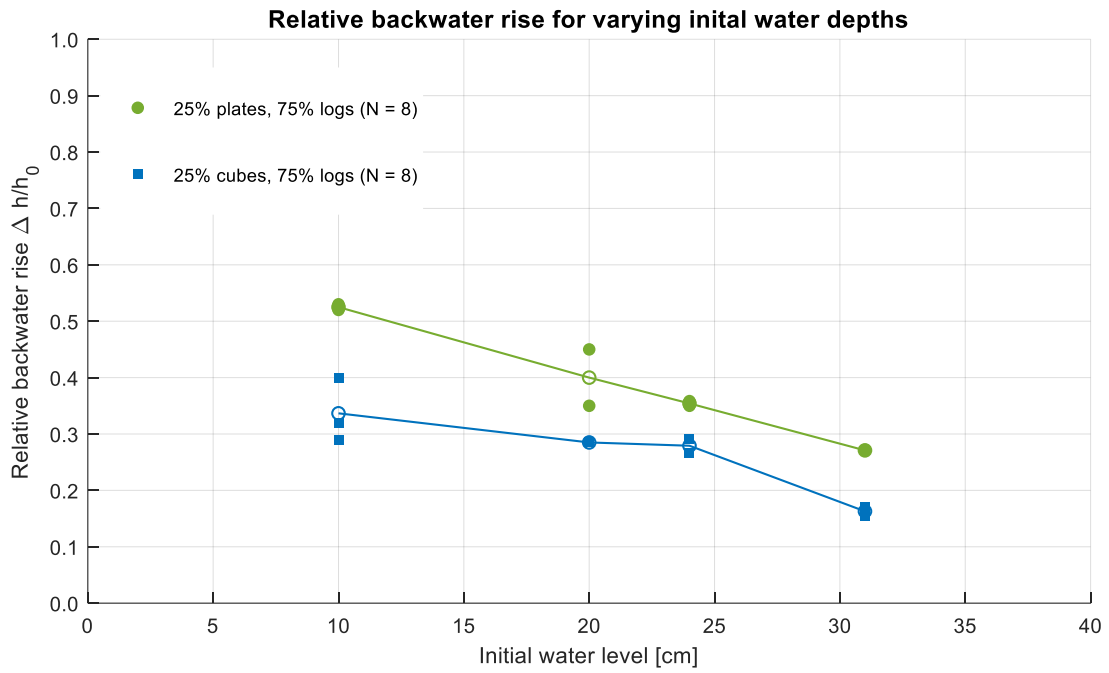


Figure 18: Relative Backwater rise in relation to the initial water depth h_0 for the model in Liège with a scale of 1:18

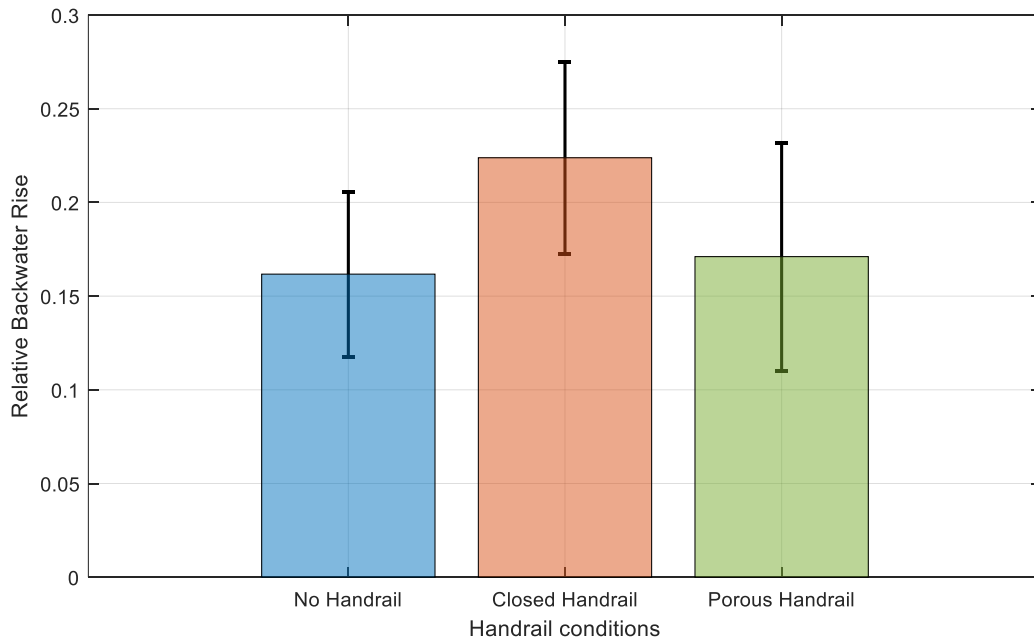


Figure 19: Relative backwater rise for different handrail designs for the tests conducted in the lab in Aachen

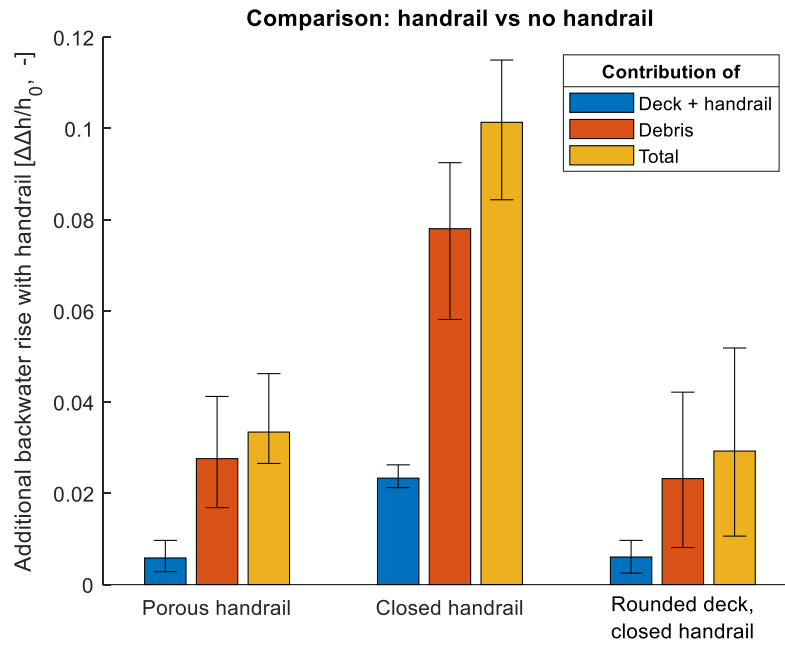


Figure 20: Relative backwater rise for different handrail designs, compared to a bridge without handrail. Data Delft, $Fr_0=0.15$, h_0 near the top of the handrail. NB: this figure also plots backwater rise by the bridge itself, in all other plots backwater rise purely refers to backwater rise from debris.

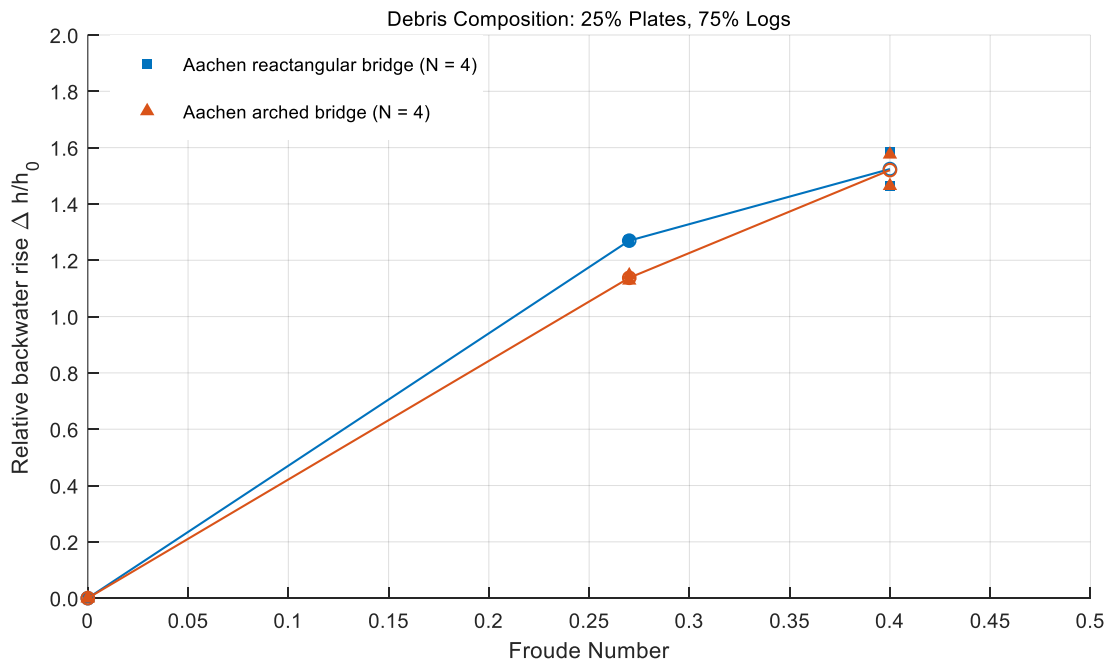


Figure 21: Relative backwater rise for bridges with rectangular and arched opening shape in the flume in Aachen

4 Design recommendations and operational procedures

4.1 Bridge design

Based on both, field observations and experimental modelling, the first recommendation for bridge design is to limit potential interactions between the bridge and debris, i.e. to limit the number of bridge elements or place them out of reach of debris. First, this means limiting the number of piers, thereby maximising the span width. This is supported by previous studies, which report that small span widths increase accumulation probability and volume (Bocchiola et al., 2008; Diehl, 1997; Lange & Bezzola, Zürich, 2006; Schmocker & Hager, 2011). Through our experiments, where blockage without piers was very difficult to achieve; and through the field analysis of the 2021 floods, which quantifies these effects, it is shown that, bridges with span widths below 10 m were especially at risk of collecting large debris accumulations. Second, a high deck is recommended, such that extreme water levels and debris do not reach the deck. Hereto, expected extreme water levels should be investigated during design phase, based on hydraulic modelling and historical records. For the studied bridges clogged during the 2021 flood, two-third of the bridges experienced water levels higher than the bridge deck. Of these bridges, the average flooding height above the deck was 1.7 meters, so any new bridges should ideally be built substantially higher. Apart from decreasing debris blockage, this would additionally decrease the risk of the bridge being unusable (flooded) during floods, the bridge being damaged or destroyed by floods, and of backwater rise due to the deck structure itself (a submerged deck creates flow resistance, irrespective of debris). Alternatively, a movable bridge could be implemented, similar to bridges that can be raised or opened to allow tall ships to pass. This has for example been implemented in Saltina (Switzerland), where a lifting bridge was constructed to allow flood peak flows to pass through the city center (Schädler, 2008).

As an additional precaution, or when the recommendations above are not implementable, it is advised to design individual bridge elements such that debris blockage, backwater rise from debris and backwater rise from the bridge itself are minimized. For the handrail, a porous handrail is advised over a solid handrail (wall). The experiments showed that this decreases both backwater rise due to the bridge itself (because water can flow through the handrail) and backwater rise from debris. In addition, debris at solid handrails can sometimes have a limited effect at first, and then suddenly cause substantial backwater rise when the debris volume increases, compared to more gradual backwater rise at porous handrails. This more gradual behaviour improves predictability and thereby decision-making during floods. However, while porous handrails decrease the *effect* of debris blockage, the *probability* of blockage increases, from debris interlocking with the handrail (Schmocker & Hager, 2011). So, from the perspective of hydraulics and debris blockage, a bridge without handrail would be ideal. As shown by the experiments, this facilitates debris to pass *over* the bridge during high water levels, thus decreasing debris blockage and backwater rise during extreme water levels. Given safety risks for traffic, a bridge without handrails seems unlikely in practice. However, the same results may be achieved by a collapsible handrail, that is removed or collapsed when a bridge is about to be flooded. This would require further study of possible structural implementations and operational procedures, but this seems worthwhile given the potential benefits for debris blockage.

Looking at the bridge deck, a slim, streamlined bridge deck is recommended. From a hydraulic perspective, a thick bridge deck forms the same obstacle as a normal deck with solid-walled railings. Accordingly, thinner decks would both decrease the backwater rise from the deck (once submerged) and from debris. A streamlined deck, with a rounded frontal area, was shown in the experiments to offer the same

advantages. In addition, this streamlining makes it easier for debris to be pulled under the bridge and be transported downstream, decreasing the probability of debris blockage (Schmocker & Hager, 2011). Potentially, a low bridge deck could be an out-of-the-box solution to limit debris blockage, especially in combination with a collapsible handrail. Here, the rationale is to place the deck at such a height above the bed, that the deck is (just) high enough not to be flooded during normal conditions, but that extreme water levels clearly exceed the bridge deck. Hence, during extreme conditions, when floating debris is most likely to occur, debris can pass over the structure instead of being blocked. However, the sacrifice of bridge usability during high waters for the mitigation of debris problems means this solution is limited to non-essential bridges, e.g. locations where other nearby bridges remain open for (evacuation and emergency) traffic during floods.

Lastly, it is recommended for bridge design to also take debris risks into account in the decision *if* and *where* a new bridge should be built, in addition to the concrete design recommendations described above. First, it bears consideration if a new bridge is really necessary, or if neighbouring bridges already provide adequate access over a river. And if needed, the bridge location should be chosen wisely. Backwater rise from debris increases when an accumulation is located at a hydraulic bottleneck. Hence, locations with a large river cross section (wide and/or deep river) are recommended. Flow velocities are lower here and debris is spread over a larger cross-sectional area, resulting in lower backwater rise for any given debris volume. In addition, a deeper river means a longer distance between bridge deck and river bed, decreasing the probability of blockage through logs being lodged between bridge deck and river bed. Furthermore, the surroundings of a new bridge location should ideally allow for building a high bridge deck, which as described before, significantly decreases debris blockage. A higher deck requires sufficient space in the surroundings, e.g. for a road sloping up towards the bridge, without limiting access to buildings.

4.2 Operational procedures and river basin management

Apart from optimizing bridge design, floating debris problems can also be mitigated by reducing debris generation. During the 2021 floods, approximately 50 percent of the debris volume consisted of trees. This means that decreasing the trees growing at riverbanks and floodplains would greatly reduce the potential for debris generation. However, given the environmental, ecological, social and scenic value of trees, large-scale removal of trees is not recommended. Nonetheless, limited removal of trees at known bank erosion hotspots, where floods are especially likely to uproot trees and entrain them in the river, would be helpful. Alternatively, bank erosion protection measures may be taken to prevent uprooting of trees. Furthermore, rules to limit the storage of cut trees for lumber in flood-prone areas could be very useful. Next, several of the large accumulations in Germany contained a substantial number of caravans. Here, improved early warning systems and evacuation plans for campsites, possibly combined with stricter rules on the start of evacuation, could greatly reduce the risk of mass entrainment of caravans into the river.

Another river basin management solution is the implementation of debris retention racks. These structures collect debris from the river, decreasing debris accumulation at bridges. Construction options vary from a row of poles to nets or floating booms (see Bradley et al., 2005; Horiguchi et al., 2015; Schmocker & Hager, 2013; Schmocker & Weitbrecht, 2013). For the study area, the developed bridge clogging database could help to determine potential locations for debris racks, by identifying in which regions debris accumulation was most extreme. Of course, the need for debris retention structures also depends on the consequences of these accumulations, i.e. backwater rise, inundation and resulting damage.

Lastly, risk from debris accumulation should explicitly be considered in operational water management. Both the observations during the 2021 flood and the experimental observations show that debris are capable of causing substantial backwater rise. This backwater rise is exacerbated in urbanized environments, where heterogeneous mixtures with building rubble were experimentally shown to be able to create twice as much backwater rise. This should be taken into account in risk analysis. For example, when creating flood hazard maps, it would be useful to make an inundation map based on the expected water level during e.g. a 100-year flood *with bridge clogging*, in addition to the conventional map based on a fully functional water system without clogging. These maps would be useful for general risk assessment, but especially also during floods, in order to quickly assess consequences once debris accumulation occurs, and take appropriate (evacuation) decisions. However, this approach would need tools to estimate the volumes of debris to be expected during floods especially within the vicinity of settlements, which are currently not available.

To include debris effects in inundation maps, the backwater rise equations by Schalko could be used (for a computational example, see Schalko, 2018, Ch. 6). In urbanized areas, the expected backwater rise should approximately be doubled, to reflect the conclusion of this project that heterogeneous debris mixtures with plates cause approximately twice the backwater rise of homogeneous natural debris mixtures. To implement this backwater rise numerically in hydraulic river models, the method of Macchione and Lombardo (2021) could be used, who determined the equivalent bottom roughness for a given accumulation and backwater rise. For the expected accumulation volume (which is required by Schalko's formulas to predict backwater rise) a first approximation would be to use accumulation volumes as documented in our database. At a higher level of detail, potential debris generation in the surroundings could be taken into account. For natural, forested environments, Schalko (2018, Ch. 2) and Bundesamt für Umwelt (2019) provided an overview of methods to estimate debris generation (often called Large Wood instead of debris in that context). For more urbanized areas, a more detailed study of the 2021 flood would be useful, to link land use, inundation depths and flow velocities to accumulated debris volumes.

The backwater rise and increased inundation upstream of clogged bridges has wider consequences. An increase in flooded area and inundation depth directly increases flood damage. Therefore, effects from debris accumulation should be included in flood damage estimates. Moreover, debris affects the propagation of a flood through a catchment area, through the additional water retention behind debris accumulations. This catchment-wide effect of local debris accumulations should be considered in the hydrological models that trigger early warning systems.

Lastly, logistic implications of debris for disaster risk management should be considered. The backwater rise and increased inundation described above may not only require faster evacuation, but also limit evacuation and emergency services by flooding or damaging roads or bridges. These factors should be taken into account in flood risk maps and evacuation plans. Also, damaged bridges can limit disaster relief and reconstruction efforts after a flood. Overall, these risks of interrupted bridge access determine, together with the availability of alternative routes, how critical it is for a specific bridge to remain accessible during floods. Hence, they should be studied carefully for existing bridges, as well as be taken into account when deciding how resilient to flooding and debris accumulation any new bridge design should be.

References

- Bauwens, A., Sohier, C., & Degré, A. (2011). Hydrological response to climate change in the Lesse and the Vesdre catchments: contribution of a physically based model (Wallonia, Belgium). *Hydrology and Earth System Sciences*, 15(6), 1745–1756. <https://doi.org/10.5194/hess-15-1745-2011>
- Bocchiola, D., Rulli, M. C., & Rosso, R. (2008). A flume experiment on the formation of wood jams in rivers. *Water Resources Research*, 44(2), Article 2006WR005846. <https://doi.org/10.1029/2006WR005846>
- Bruwier, M., Ercicum, S., Piroton, M., Archambeau, P., & Dewals, B. J. (2015). Assessing the operation rules of a reservoir system based on a detailed modelling chain. *Natural Hazards and Earth System Sciences*, 15(3), 365–379. <https://doi.org/10.5194/nhess-15-365-2015>
- Bundesamt für Umwelt (Ed.). (2019). *Schwemmholz in Fliessgewässern. Ein praxisorientiertes Forschungsprojekt.* (Umwelt-Wissen No. 1910). Bern.
- Burghardt, L [Lisa], Schüttrumpf, H [Holger], Wolf, S [Stefanie], & Klopries, E.-M. (2022). Analyse der Schäden an Brückenbauwerken in Folge des Hochwassers 2021 an der Ahr. *Wasser Und Abfall*, 24(11), 12–17. <https://doi.org/10.1007/s35152-022-1346-x>
- Deutsches Komitee Katastrophenvorsorge e.V. (Ed.). (2022). *Die Flutkatastrophe im Juli 2021 in Deutschland: Ein Jahr danach: Aufarbeitung und erste Lehren für die Zukunft* (DKKV-Schriftenreihe No. 62). Bonn.
- Diehl, T. H. (April 1997). *Potential Drift Accumulation at Bridges*. Nashville.
- Talsperren in Deutschland.* (2013). Springer Vieweg. <http://ifb.bsz-bw.de/bsz380513021rez-1.pdf>
- Koks, E. E., van Ginkel, K. C. H., van Marle, M. J. E., & Lemnitzer, A [Anne] (2022). Brief communication: Critical infrastructure impacts of the 2021 mid-July western European flood event. *Natural Hazards and Earth System Sciences*, 22(12), 3831–3838. <https://doi.org/10.5194/nhess-22-3831-2022>
- Korswagen, P., Selvam, H., Oetjen, J., & Wüthrich, D. (2022). *Post-flood field survey of the Ahr Valley (Germany)*. <https://doi.org/10.4121/19222656>
- Land NRW (Ed.). (2023, March 15). *ELWAS-WEB: Oberflächengewässer - Pegel*. <https://www.elwasweb.nrw.de>
- Landesamt für Umwelt Rheinland-Pfalz. (n. d.). *Die Ahr*. Retrieved October 31, 2023, from <https://wasser.rlp-umwelt.de/servlet/is/1210/>
- Landesamt für Umwelt Rheinland-Pfalz (Ed.). (2022). *Bericht: Hochwasser im Juli 2021*. Mainz. https://lfu.rlp.de/fileadmin/lfu/Wasserwirtschaft/Ahr-Katastrophe/Hochwasser_im_Juli2021.pdf
- Lange, D., & Bezzola, G. R. (Zürich, 2006). *Schwemmholz: Probleme und Lösungsansätze* (Mitteilungen No. 188). Versuchsanstalt für Wasserbau, Hydrologie und Glaziologie, ETH-Zentrum. <https://ethz.ch/content/dam/ethz/special-interest/baug/vaw/vaw-dam/documents/das-institut/mitteilungen/2000-2009/188.pdf>
- Lemnitzer, A [A.], Gardner, M., Stark, N., Nichols, E., George, M., Müller, J., Stamm, J., Zimmermann, R., Schüttrumpf, H [H.], Wolf, S [S.], Burghardt, L [L.], & Klopries, E. (2023). Geotechnical and Geo-Environmental Damage and its Impacts on Critical Community Infrastructure during the 2021 Western European Floods: The Case Study of Altenahr, Germany Geotechnical and Geo-Environmental Damage and its. In International Society for Soil Mechanics and Geotechnical Engineering (Chair), *9th International Congress on Environmental Geotechnics*. Symposium conducted at the meeting of University of California at Berkeley, Chania, Greece. <https://www.issmge.org/uploads/publications/116/117/ICEG2023-428.pdf>
- Lucía, A., Comiti, F., Borga, M., Cavalli, M., & Marchi, L. (2015). Dynamics of large wood during a flash flood in two mountain catchments. *Natural Hazards and Earth System Sciences*, 15(8), 1741–1755. <https://doi.org/10.5194/nhess-15-1741-2015>

- Macchione, F., & Lombardo, M. (2021). Roughness-Based Method for Simulating Hydraulic Consequences of Both Woody Debris Clogging and Breakage at Bridges in Basin-Scale Flood Modeling. *Water Resources Research*, 57(12), Article e2021WR030485. <https://doi.org/10.1029/2021WR030485>
- Ministerium für Klimaschutz, Umwelt, Energie und Mobilität Rheinland-Pfalz. (n. d.). *Die Ahr*. Retrieved March 31, 2023, from <https://wasser.rlp-umwelt.de/servlet/is/1210/>
- Mohr, S., Ehret, U., Kunz, M., Ludwig, P., Caldas-Alvarez, A., Daniell, J. E., Ehmele, F., Feldmann, H., Franca, M. J., Gattke, C., Hundhausen, M., Knippertz, P., Küpfer, K., Mühr, B., Pinto, J. G., Quinting, J., Schäfer, A. M., Scheibel, M., Seidel, F., & Wisotzky, C. (2023). A multi-disciplinary analysis of the exceptional flood event of July 2021 in central Europe – Part 1: Event description and analysis. *Natural Hazards and Earth System Sciences*, 23(2), 525–551. <https://doi.org/10.5194/nhess-23-525-2023>
- Rusyda, M. I., Kusukubo, M., Maricar, M. F., Ikematsu, S., & Hashimoto, H. (2014). Woody debris accumulation during the flood event in the Nayoshi River, Tsuwano Town, Japan. In *Proceedings of the 19th IAHR-APD Congress*, Hanoi, Vietnam.
- Schädler, B. (2008, June 24). Hochwasserschutz-Strategie im Gebirgsland Schweiz. In *Beiträge zum Symposium Klimaänderung - Was kann die Wasserwirtschaft tun?*
- Schäfer, A., Mühr, B., Daniell, J., Ehret, U., Ehmele, F., Küpfer, K., Brand, J., Wisotzky, C., Skapski, J., Rentz, L., Mohr, S., & Kunz, M. (2021). *Hochwasser Mitteleuropa, Juli 2021 (Deutschland) : 21. Juli 2021 – Bericht Nr. 1 „Nordrhein-Westfalen & Rheinland-Pfalz“*. CEDIM Forensic Disaster Analysis (FDA) Group. <https://doi.org/10.5445/IR/1000135730>
- Schalko, I. (2018). *Modeling Hazards Related to Large Wood in Rivers* [, ETH Zurich]. DataCite.
- Schmocker, L., & Hager, W. H. (2011). Probability of Drift Blockage at Bridge Decks. *Journal of Hydraulic Engineering*, 137(4), 470–479. [https://doi.org/10.1061/\(ASCE\)HY.1943-7900.0000319](https://doi.org/10.1061/(ASCE)HY.1943-7900.0000319)
- Steeb, N., Rickenmann, D., Badoux, A., Rickli, C., & Waldner, P. (2017). Large wood recruitment processes and transported volumes in Swiss mountain streams during the extreme flood of August 2005. *Geomorphology*, 279, 112–127. <https://doi.org/10.1016/j.geomorph.2016.10.011>
- Tubaldi, E., White, C. J., Patelli, E., Mitoulis, S. A., Almeida, G. de, Brown, J., Cranston, M., Hardman, M., Koursari, E., Lamb, R., McDonald, H., Mathews, R., Newell, R., Pizarro, A., Roca, M., & Zonta, D. (2022). Invited perspectives: Challenges and future directions in improving bridge flood resilience. *Natural Hazards and Earth System Sciences*, 22(3), 795–812. <https://doi.org/10.5194/nhess-22-795-2022>
- Wasserverband Eifel-Rur (Ed.). (n. a.a). *Die Inde*. <https://wver.de/fluss/die-inde/>
- Wasserverband Eifel-Rur (Ed.). (n. a.b). *Die Vicht*. <https://wver.de/fluss/die-vicht/>
- Zanke, U. (2013). *Hydraulik für den Wasserbau* (3. Aufl.). Springer Vieweg.

Appendices

Appendix 1: Parameter description of field observation database

This appendix explains in detail which parameters were collected on the field data of bridges clogged during the flood event in 2021 (Chapter 2) and documented in the resulting database. The database is divided in six sections, encompassing around 60 parameters. The content of each database section is depicted below, with the meaning, value and formatting of each parameter.

Encoding section

This section shows the unique identifier of the bridge in the database and identifies by whom and when the encoding has been done.

Table 1.1 : Parameters describing encoding

Data name	Meaning	Values and formatting
<i>ID</i>	Five digits unique identifier of the structure in the database	10000 to 19999 → structures in Germany 20000 to 29999 → structures in The Netherlands 30000 to 39999 → structures in Belgium
<i>Institution</i>	Name of the institution responsible for the bridge encoding	<i>RWTH, TUDelft or ULiège</i>
<i>Encoder</i>	Initials of the researcher responsible for the encoding	
<i>Date</i>	Date of encoding validation by the <i>Encoder</i>	[DD/MM/YYYY]

Location section

This section contains the information needed to identify the structure and locate it spatially.

Table 1.2 : Parameters describing structure location

Data name	Meaning	Values, formatting and units
<i>Type</i>	Type of structure	<i>Bridge, Railway bridge or Culvert</i>
<i>Year</i>	Year of structure first commissioning	[YYYY]
<i>Year comment</i>	Possible comment related to year of commissioning	
<i>River</i>	Name of the river on which the structure has been erected	
<i>Municipality</i>	Name of the municipality in which the structure is located	
<i>Structure / street name</i>	Name of the structure or of the street passing over it	
<i>EPSG</i>	EPSG code of the coordinate reference system	Number between 1024 and 32767

<i>X reg</i>	X coordinate of the structure center in EPSG coordinate system	
<i>Y reg</i>	Y coordinate of the structure center in EPSG coordinate system	
<i>Lat</i>	Latitude of the structure center	[° ' " N]
<i>Long</i>	Longitude of the structure center	[° ' " E]
<i>Curv</i>	Curvilinear abscissa of the structure along river axis, counted from the river mouth	[m]
<i>Riverbed elevation</i>	Minimum elevation of the riverbed below the structure	[m]
<i>Upstream river shape</i>	Shape of the riverbed upstream of the structure	<p><i>Straight:</i> when a straight line directed upstream whose length is five times the river width and whose origin is on the center of the structure upstream face does not cross a riverbank.</p> <p><i>Curved right:</i> when a straight line directed upstream whose length is five times the river width and whose origin is on the center of the structure upstream face crosses the left riverbank.</p> <p><i>Curved left:</i> when a straight line directed upstream whose length is 5 times the river width and whose origin is on the center of the structure upstream face crosses the right riverbank.</p>

Structure section

This section contains a geometric description of the structure.

Table 1.3 : Parameters describing structure geometry

Data name	Meaning	Values and formatting
<i>Opening(s) shape</i>	Shape of the opening(s) through which the river flows	<i>Rectangular or Arched</i>
<i>Width</i>	Horizontal dimension of the structure perpendicular to its length	[m]
<i>Length</i>	Horizontal dimension of the structure from bank to bank	[m]
<i>Slope</i>	Slope of the structures upper face, from right to left bank, positive in clockwise direction.	[%]
<i>Angle</i>	Angle between structure width and left riverbank, positive in clockwise direction	[°]
<i>Thickness</i>	Deck thickness at opening center	[m]

<i>Elevation</i>	Center elevation of the structure upper face	[m]
<i>River cross-section</i>	Shape of the river cross-section through the structure	<i>Regular</i> : symmetric rectangular or trapezoidal cross section <i>Irregular</i> : any other cross section shape
<i>Abutments</i>	Abutment(s) on the riverbank	<i>Present</i> or <i>Absent</i>
<i>Number of pier(s)</i>	Number of piers in the riverbed. Abutments are not considered as piers	
<i>Pier(s) width</i>	Maximum dimension of the pier(s) perpendicular to riverbed axis	[m]
<i>Distance between piers</i>	Distance between piers from left to right bank	Number of pier(s) + 1 value(s) [m]-...-[m]
<i>Min distance</i>	Minimum distance between two piers or abutments	[m]
<i>Max distance</i>	Maximum distance between two piers or abutments	[m]
<i>Pier(s) shape</i>	Shape of pier(s) nose facing the flow	<i>Circular</i> : circular pier <i>Rounded</i> : rounded nose <i>Sharp</i> : triangular nose <i>Square</i> : flat nose (no profiling)
<i>Pier(s) protrusion</i>	Distance between the pier upstream nose and the bridge deck	[m]
<i>Handrail material</i>	Material of the handrail	<i>Stone, metal, mixed</i> (stone and metal) or <i>other</i>
<i>Handrail height</i>	Height of the handrail	[m]
<i>Handrail porosity</i>	Estimated ratio of openings area to solid area in handrail	<i>Total</i> : no handrail <i>High</i> : handrail made of thin elements with large spacing <i>Medium</i> : handrail made of thin elements with low spacing <i>Low</i> : handrail made of broad elements with low spacing <i>No porosity</i> : continuous wall
<i>Structure damage</i>	Level of damage to the structure observed after July 2021 event	<i>No</i> : no damage <i>Weak</i> : small and limited extend damage without compromising use and stability <i>Moderate</i> : several local damage without compromising use and stability <i>Strong</i> : damage preventing use of the structure but not compromising its stability <i>Complete</i> : the structure is no more present, or integrity is compromised

Flood event at the structure

This section presents main flow conditions at the structure during July 2021 event.

Table 1.4 : Parameters describing flood conditions at structure location

Data name	Meaning	Values and formatting
<i>Type of flow</i>	Flow condition at the structure	<i>Pressurized</i> : water level is equal to structure elevation <i>Free surface</i> : water level is below structure elevation <i>Mixed</i> : water level is above structure elevation
<i>Discharge</i>	Max flow discharge in the river at the structure location during the event	[m ³ /s]
<i>Max water elevation</i>	Maximum water elevation observed at the structure during the event	[m]
<i>Max water depth</i>	Difference between <i>max water elevation</i> and <i>riverbed elevation</i>	[m]
<i>Flow width</i>	Flow width at the structure location during the event	[m]

Deposit

Description of the debris deposit blocked at the structure.

Table 1.5 : Parameters describing the deposit blocked at the structure

Data name	Meaning	Values and formatting
<i>Clogging</i>	Debris accumulation at the structure during the event	<i>Yes</i> : yes with certainty <i>No</i> : no with certainty <i>No information</i> : no clue based on available information
<i>Carpet</i>	Continuous and compact accumulation of debris just upstream of the structure	<i>Yes</i> : yes with certainty <i>No</i> : no with certainty <i>No information</i> : no clue based on available information
<i>Total length</i>	Max dimension parallel to river axis of debris accumulation area upstream of the structure	[m]
<i>Total width</i>	Max dimension normal to river axis of debris accumulation area upstream of the structure	[m]
<i>Total height</i>	Max visible vertical dimension of debris accumulation area upstream of the structure	[m]
<i>Carpet length</i>	Max dimension parallel to river axis of the carpet	[m]

<i>Carpet width</i>	Max dimension normal to river axis of the carpet	[m]
<i>Carpet height</i>	Max visible vertical dimension of the carpet	[m]
<i>Volume</i>	Visible volume of debris blocked upstream of the structure	[m ³]
<i>Location at structure</i>	Location of the debris blocked upstream of the structure	<p><i>Whole width</i>: debris accumulation occupies at least 80% of the structure length</p> <p><i>Right bank</i>: debris accumulation is less than 80% of the structure length and is mainly on right bank of the structure</p> <p><i>Left bank</i>: debris accumulation is less than 80% of the structure length and is mainly on left bank of the structure</p> <p><i>Center</i>: debris accumulation is less than 80% of the structure length and is centered at the structure</p> <p><i>Pier(s)</i>: debris accumulation is limited and only at pier(s)</p> <p><i>Handrail</i>: debris accumulation is only at handrail</p>

Main debris content

Characteristics of the main elements constituting debris accumulation: percentage in volume and type of the maximum five types of elements constituting most of the accumulation.

Table 1.6: Parameters describing the debris constituting the deposit blocked at the structure

Data name	Meaning	Values and formatting
<i>Main trunk presence</i>	Presence of a large trunk (compared to structure opening) blocked in structure opening	<p><i>Yes</i>: yes with certainty</p> <p><i>No</i>: no with certainty</p> <p><i>No information</i>: unknown based on available information</p>
<i>Id main type i</i>	Type of elements (<i>i</i> from 1 to maximum 5)	<p>20: Natural wood</p> <p>21: Anthropogenic wood</p> <p>22: Plastic container</p> <p>23: Metal container</p> <p>24: Vehicle</p> <p>25: Household items</p> <p>26: Industry items</p> <p>27: Building rubble</p> <p>30: Other</p>
<i>Volume percentage i</i>	Volume in percent of elements of <i>main type i</i> compared to <i>Volume</i>	[%]

All the pictures used to estimate the parameters values are identified with a six digits IDs whose five first digits are the structure ID ones and the last digit ranges from 0 to 9 (maximum 10 pictures per structure).

Appendix 2: Detailed composition of different debris mixtures

Logs	Cubes	Plates	Number of batches	Number of cubes per batch	Height of plates per batch	Logs [length in cm]								Volume per batch [dm ³]
						80	70	60	50	40	30	20	10	
100	0	0	40	0	0	3/4	1 1/4	2	3	5	10	20	50	4.751
75	25	0	30	33	0	3/4	1 1/4	2	3	5	10	20	50	6.355
50	50	0	20	65	0	3/4	1 1/4	2	3	5	10	20	50	9.490
75	0	25	30	0	25.33	3/4	1 1/4	2	3	5	10	20	50	6.271
50	0	50	40	0	38	3/8	5/8	1	1 1/2	2 1/2	5	10	25	4.656
60	20	20	24	27	25.33	3/4	1 1/4	2	3	5	10	20	50	7.911
40	30	30	32	40	28.5	3/8	5/8	1	1 1/2	2 1/2	5	10	25	5.908

Appendix 3: Density measurements for the debris components in wet and dry state

	Length [in cm]	Volume [dm ³]	Mean density dry [kg/dm ³]	Mean density wet [kg/dm ³]
Logs	10	0.002	0.510	0.710
	20	0.016	0.424	0.438
	30	0.053	0.479	0.453
	40	0.126	0.558	0.556
	50	0.245	0.610	0.596
	60	0.424	0.636	0.675
	70	0.673	0.649	0.654
	80	1.005	0.654	0.675
Plates	-	0.012	0.898	0.944
Cubes	-	1.458	0.502	0.557

Appendix 4: Overview of all the tests conducted in the three laboratories

File name

Lab Liege

Large flume (1.2 m wide), debris mixture

Methods

B1_R_2P_F028_h27_100L_no80cm_1HR_R1_52L
 B1_R_2P_F028_h27_100L_1HR_small_batch_R1_57L
 B1_R_2P_F028_h27_100L_1HR_orientation_parallel_R1_57L
 B1_R_2P_F028_h27_100L_50to80cm_1HR_R1_57L
 B1_R_2P_F028_h27_100L_10to40cm_plus_ini_1HR_R1_60L
 B1_R_2P_F028_h27_100L_1HR_10min_R_57L

Debris mixtures: 100% logs

B1_R_2P_F028_h27_100L_1HR_R1_57L
 B1_R_2P_F028_h27_100L_1HR_R2_57L
 B1_R_2P_F028_h27_100L_1HR_R3_57L
 B1_R_2P_F028_h27_100L_1HR_R4_190L
 B1_R_2P_F028_h27_100L_1HR_R5_sensor1incomplete_190L
 B1_R_2P_F028_h27_100L_1HR_R6_190L

25% cubes

B1_R_2P_F028_h27_25C_75L_1HR_R1_190L
 B1_R_2P_F028_h27_25C_75L_1HR_R2_190L
 B1_R_2P_F028_h27_25C_75L_1HR_R3_190L

50% cubes

B1_R_2P_F028_h27_50C_50L_1HR_R1_57L
 B1_R_2P_F028_h27_50C_50L_1HR_R2_190L
 B1_R_2P_F028_h27_50C_50L_1HR_R3_190L
 B1_R_2P_F028_h27_50C_50L_1HR_R4_190L

25% plates

B1_R_2P_F028_h27_25P_75L_1HR_R1_139L
 B1_R_2P_F028_h27_25P_75L_1HR_R2_127L
 B1_R_2P_F028_h27_25P_75L_1HR_R3_139L

50% plates

B1_R_2P_F028_h27_50P_50L_1HR_R1_190L
 B1_R_2P_F028_h27_50P_50L_1HR_R2_190L
 B1_R_2P_F028_h27_50P_50L_1HR_R3_176L
 B1_R_2P_F028_h27_50P_50L_1HR_R4_124L

20% plates and cubes

B1_R_2P_F028_h27_20P_20C_60L_1HR_R1_190L
 B1_R_2P_F028_h27_20P_20C_60L_1HR_R2_190L
 B1_R_2P_F028_h27_20P_20C_60L_1HR_R3_158L

30% plates and cubes

B1_R_2P_F028_h27_30P_30C_40L_1HR_R1_190L
 B1_R_2P_F028_h27_30P_30C_40L_1HR_R2_190L
 B1_R_2P_F028_h27_30P_30C_40L_1HR_R3_190L

Large flume (1.2 m wide), rest

B1_R_2P_F013_h27_25C75L_1HR_R1_80L
 B1_R_2P_F013_h27_25C75L_1HR_R2_80L
 B1_R_2P_F013_h27_25P75L_1HR_R1_80L
 B1_R_2P_F013_h27_25P75L_1HR_R2_80L

B1_R_2P_F027_h27_25C75L_1HR_R1_80L
 B1_R_2P_F027_h27_25C75L_1HR_R2_80L
 B1_R_2P_F027_h27_25P75L_1HR_R1_80L
 B1_R_2P_F027_h27_25P75L_1HR_R2_80L
 B1_A_2P_F027_h27_25C75L_2HR_R1_80L
 B1_A_2P_F027_h27_25C75L_2HR_R2_80L
 B1_A_2P_F027_h27_25P75L_2HR_R1_80L
 B1_A_2P_F027_h27_25P75L_2HR_R2_80L
 B1_A_2P_F028_h34_25C75L_2HR_R1_80L
 B1_A_2P_F028_h34_25C75L_2HR_R2_80L
 B1_A_2P_F028_h34_25P75L_2HR_R1_80L
 B1_A_2P_F028_h34_25P75L_2HR_R2_80L
 B1_A_2P_F040_h30_25C75L_2HR_R1_80L
 B1_A_2P_F040_h30_25C75L_2HR_R2_80L
 B1_A_2P_F040_h30_25P75L_2HR_R1_80L

Small flume (1m wide), 1 pier

Froude 0.2

B2_R_1P_F020_h37,5_25C75L_OHR_R1_50L
 B2_R_1P_F020_h37,5_25P75L_OHR_R1_50L

Froude 0.27

B2_R_1P_F027_h10_25C75L_OHR_R1_50L
 B2_R_1P_F027_h10_25C75L_OHR_R2_50L
 B2_R_1P_F027_h10_25C75L_OHR_R3_50L
 B2_R_1P_F027_h10_25P75L_OHR_R1_50L
 B2_R_1P_F027_h10_25P75L_OHR_R2_50L
 B2_R_1P_F027_h20_25C75L_OHR_R1_50L
 B2_R_1P_F027_h20_25C75L_OHR_R2_50L
 B2_R_1P_F027_h20_25P75L_OHR_R1_50L
 B2_R_1P_F027_h20_25P75L_OHR_R2_50L
 B2_R_1P_F027_h24_25C75L_OHR_R1_50L
 B2_R_1P_F027_h24_25C75L_OHR_R2_50L
 B2_R_1P_F027_h24_25P75L_OHR_R1_50L
 B2_R_1P_F027_h24_25P75L_OHR_R2_50L
 B2_R_1P_F027_h31_25C75L_OHR_R1_50L
 B2_R_1P_F027_h31_25C75L_OHR_R2_50L
 B2_R_1P_F027_h31_25P75L_OHR_R1_50L
 B2_R_1P_F027_h31_25P75L_OHR_R2_50L

Froude 0.4

B2_R_1P_F040_h10_25C75L_OHR_R1_50L
 B2_R_1P_F040_h10_25C75L_OHR_R2_50L
 B2_R_1P_F040_h10_25C75L_OHR_R3_50L
 B2_R_1P_F040_h10_25P75L_OHR_R1_50L
 B2_R_1P_F040_h10_25P75L_OHR_R2_50L
 B2_R_1P_F040_h20_25C75L_OHR_R1_50L
 B2_R_1P_F040_h20_25C75L_OHR_R2_50L
 B2_R_1P_F040_h20_25P75L_OHR_R1_50L
 B2_R_1P_F040_h20_25P75L_OHR_R2_50L
 B2_R_1P_F040_h24_25C75L_OHR_R1_50L
 B2_R_1P_F040_h24_25C75L_OHR_R2_50L
 B2_R_1P_F040_h24_25P75L_OHR_R1_50L
 B2_R_1P_F040_h24_25P75L_OHR_R2_50L

Froude 0.6

B2_R_1P_F060_h10_25C75L_OHR_R1_50L
 B2_R_1P_F060_h10_25C75L_OHR_R2_50L
 B2_R_1P_F060_h10_25C75L_OHR_R3_50L
 B2_R_1P_F060_h10_25P75L_OHR_R1_50L
 B2_R_1P_F060_h10_25P75L_OHR_R2_50L
 B2_R_1P_F060_h20_25C75L_OHR_R1_50L
 B2_R_1P_F060_h20_25C75L_OHR_R2_50L
 B2_R_1P_F060_h20_25P75L_OHR_R1_50L
 B2_R_1P_F060_h20_25P75L_OHR_R2_50L

Small flume (1 m wide), 2 piers**Froude 0.13**

B2_R_2P_F013_h21,1_25C75L_OHR_R1_50L
 B2_R_2P_F013_h21,1_25C75L_OHR_R2_50L
 B2_R_2P_F013_h21,1_25C75L_OHR_R3_50L
 B2_R_2P_F013_h21,1_25C75L_OHR_R4_50L
 B2_R_2P_F013_h21,1_25P75L_OHR_R1_50L
 B2_R_2P_F013_h21,1_25P75L_OHR_R2_50L
 B2_R_2P_F013_h21,1_25P75L_OHR_R3_50L
 B2_R_2P_F013_h21,1_25P75L_OHR_R4_50L

Froude 0.2

B2_R_2P_F020_h37,5_25C75L_OHR_R1_50L
 B2_R_2P_F020_h37,5_25P75L_OHR_R1_50L

Froude 0.27

B2_R_2P_F027_h10_25C75L_OHR_R1_50L
 B2_R_2P_F027_h10_25C75L_OHR_R2_50L
 B2_R_2P_F027_h10_25C75L_OHR_R3_50L
 B2_R_2P_F027_h10_25C75L_OHR_R4_50L
 B2_R_2P_F027_h10_25P75L_OHR_R1_50L
 B2_R_2P_F027_h10_25P75L_OHR_R2_50L
 B2_R_2P_F027_h15_25C75L_OHR_R1_50L
 B2_R_2P_F027_h15_25C75L_OHR_R2_50L
 B2_R_2P_F027_h15_25P75L_OHR_R1_50L
 B2_R_2P_F027_h15_25P75L_OHR_R2_50L
 B2_R_2P_F027_h20_25C75L_OHR_R1_50L
 B2_R_2P_F027_h20_25C75L_OHR_R2_50L
 B2_R_2P_F027_h20_25P75L_OHR_R1_50L
 B2_R_2P_F027_h20_25P75L_OHR_R2_50L
 B2_R_2P_F027_h21,1_25C75L_OHR_R1_50L
 B2_R_2P_F027_h21,1_25C75L_OHR_R2_50L
 B2_R_2P_F027_h21,1_25P75L_OHR_R1_50L
 B2_R_2P_F027_h21,1_25P75L_OHR_R2_50L
 B2_R_2P_F027_h24_25C75L_OHR_R1_50L
 B2_R_2P_F027_h24_25C75L_OHR_R2_50L
 B2_R_2P_F027_h24_25P75L_OHR_R1_50L
 B2_R_2P_F027_h24_25P75L_OHR_R2_50L
 B2_R_2P_F027_h31_25C75L_OHR_R1_50L
 B2_R_2P_F027_h31_25C75L_OHR_R2_50L
 B2_R_2P_F027_h31_25P75L_OHR_R1_50L
 B2_R_2P_F027_h31_25P75L_OHR_R2_50L

Froude 0.4

B2_R_2P_F040_h10_25C75L_OHR_R1_50L
 B2_R_2P_F040_h10_25C75L_OHR_R2_50L
 B2_R_2P_F040_h10_25P75L_OHR_R1_50L
 B2_R_2P_F040_h10_25P75L_OHR_R2_50L
 B2_R_2P_F040_h15_25C75L_OHR_R1_50L
 B2_R_2P_F040_h15_25C75L_OHR_R2_50L
 B2_R_2P_F040_h15_25P75L_OHR_R1_50L
 B2_R_2P_F040_h15_25P75L_OHR_R2_50L
 B2_R_2P_F040_h20_25C75L_OHR_R1_50L
 B2_R_2P_F040_h20_25C75L_OHR_R2_50L
 B2_R_2P_F040_h20_25P75L_OHR_R1_50L
 B2_R_2P_F040_h20_25P75L_OHR_R2_50L
 B2_R_2P_F040_h24_25C75L_OHR_R1_50L
 B2_R_2P_F040_h24_25C75L_OHR_R2_50L
 B2_R_2P_F040_h24_25P75L_OHR_R1_50L
 B2_R_2P_F040_h24_25P75L_OHR_R2_50L

Froude 0.6

B2_R_2P_F060_h10_25C75L_OHR_R1_50L
 B2_R_2P_F060_h10_25C75L_OHR_R2_50L
 B2_R_2P_F060_h10_25P75L_OHR_R1_50L
 B2_R_2P_F060_h10_25P75L_OHR_R2_50L
 B2_R_2P_F060_h15_25C75L_OHR_R1_50L
 B2_R_2P_F060_h15_25C75L_OHR_R2_50L
 B2_R_2P_F060_h15_25P75L_OHR_R1_50L
 B2_R_2P_F060_h15_25P75L_OHR_R2_50L
 B2_R_2P_F060_h20_25C75L_OHR_R1_50L
 B2_R_2P_F060_h20_25C75L_OHR_R2_50L
 B2_R_2P_F060_h20_25P75L_OHR_R1_50L
 B2_R_2P_F060_h20_25P75L_OHR_R2_50L

Lab Aachen

Arched bridge

Debris mixtures

G1_A_2P_F028_h27_20P20C60L_2HR_R1_190L
 G1_A_2P_F028_h27_20P20C60L_2HR_R2_190L
 G1_A_2P_F028_h27_20P20C60L_2HR_R3_190L
 G1_A_2P_F028_h27_25C75L_2HR_R1_190L
 G1_A_2P_F028_h27_25C75L_2HR_R2_190L
 G1_A_2P_F028_h27_25C75L_2HR_R3_190L
 G1_A_2P_F028_h27_25C75L_2HR_R4_76L
 G1_A_2P_F028_h27_25P75L_2HR_R1_190L
 G1_A_2P_F028_h27_25P75L_2HR_R2_190L
 G1_A_2P_F028_h27_25P75L_2HR_R3_190L
 G1_A_2P_F028_h27_30P30C40L_2HR_R1_190L
 G1_A_2P_F028_h27_30P30C40L_2HR_R2_190L
 G1_A_2P_F028_h27_30P30C40L_2HR_R3_190L
 G1_A_2P_F028_h27_50C50L_2HR_R1_190L
 G1_A_2P_F028_h27_50C50L_2HR_R2_190L
 G1_A_2P_F028_h27_50C50L_2HR_R3_190L
 G1_A_2P_F028_h27_50P50L_2HR_R1_190L
 G1_A_2P_F028_h27_50P50L_2HR_R2_190L
 G1_A_2P_F028_h27_50P50L_2HR_R3_190L

G1_A_2P_F028_h27_100L_2HR_R1_190L
G1_A_2P_F028_h27_100L_2HR_R2_190L
G1_A_2P_F028_h27_100L_2HR_R3_190L

Hydraulic conditions, Froude 0.13

G1_A_2P_F013_h27_25C75L_2HR_R1_76L
G1_A_2P_F013_h27_25P75L_2HR_R1_76L
G1_A_2P_F013_h27_25P75L_2HR_R2_76L

Froude 0.28

G1_A_2P_F028_h15,3_25C75L_2HR_R1_76L
G1_A_2P_F028_h15,3_25C75L_2HR_R2_76L
G1_A_2P_F028_h15,3_25P75L_2HR_R1_76L
G1_A_2P_F028_h15,3_25P75L_2HR_R2_76L
G1_A_2P_F028_h22_25C75L_2HR_R1_76L
G1_A_2P_F028_h22_25P75L_2HR_R1_76L
G1_A_2P_F028_h22_25P75L_2HR_R2_76L
G1_A_2P_F028_h30_25C75L_2HR_R1_76L
G1_A_2P_F028_h30_25C75L_2HR_R2_76L
G1_A_2P_F028_h30_25P75L_2HR_R1_76L
G1_A_2P_F028_h30_25P75L_2HR_R2_76L
G1_A_2P_F028_h34_25C75L_2HR_R1_76L
G1_A_2P_F028_h34_25C75L_2HR_R2_76L
G1_A_2P_F028_h34_25P75L_2HR_R1_76L
G1_A_2P_F028_h34_25P75L_2HR_R2_76L

Froude 0.4

G1_A_2P_F040_h15,3_25C75L_2HR_R1_76L
G1_A_2P_F040_h15,3_25C75L_2HR_R2_76L
G1_A_2P_F040_h15,3_25P75L_2HR_R1_76L
G1_A_2P_F040_h15,3_25P75L_2HR_R2_76L
G1_A_2P_F040_h22_25C75L_2HR_R1_76L
G1_A_2P_F040_h22_25C75L_2HR_R2_76L
G1_A_2P_F040_h22_25P75L_2HR_R1_76L
G1_A_2P_F040_h22_25P75L_2HR_R2_76L
G1_A_2P_F040_h27_25C75L_2HR_R1_76L
G1_A_2P_F040_h27_25C75L_2HR_R2_76L
G1_A_2P_F040_h27_25P75L_2HR_R1_76L
G1_A_2P_F040_h27_25P75L_2HR_R2_76L
G1_A_2P_F040_h30_25C75L_2HR_R1_76L
G1_A_2P_F040_h30_25C75L_2HR_R2_76L
G1_A_2P_F040_h30_25P75L_2HR_R1_76L
G1_A_2P_F040_h30_25P75L_2HR_R2_76L
G1_A_2P_F040_h34_25C75L_2HR_R1_76L
G1_A_2P_F040_h34_25C75L_2HR_R2_76L
G1_A_2P_F040_h34_25P75L_2HR_R1_76L
G1_A_2P_F040_h34_25P75L_2HR_R2_76L

Froude 0.5

G1_A_2P_F050_h15,3_25C75L_2HR_R1_76L
G1_A_2P_F050_h15,3_25C75L_2HR_R2_76L
G1_A_2P_F050_h15,3_25P75L_2HR_R1_76L
G1_A_2P_F050_h15,3_25P75L_2HR_R2_76L
G1_A_2P_F050_h22_25C75L_2HR_R1_76L
G1_A_2P_F050_h22_25C75L_2HR_R2_76L

G1_A_2P_F050_h22_25P75L_2HR_R1_76L
 G1_A_2P_F050_h22_25P75L_2HR_R2_76L
 G1_A_2P_F050_h27_25C75L_2HR_R1_76L
 G1_A_2P_F050_h27_25C75L_2HR_R2_76L
 G1_A_2P_F050_h27_25P75L_2HR_R1_76L
 G1_A_2P_F050_h27_25P75L_2HR_R2_76L

Rectangular bridge

Single handrail

G1_R_2P_F040_h27_25P75L_1HR_R1_76
 G1_R_2P_F040_h27_25P75L_1HR_R2_76L
 G1_R_2P_F028_h22_25C75L_1HR_R1_76L
 G1_R_2P_F028_h27_25C75L_1HR_R1_76L
 G1_R_2P_F028_h27_25C75L_1HR_R2_76L
 G1_R_2P_F028_h27_25P75L_1HR_R1_76L
 G1_R_2P_F028_h27_25P75L_1HR_R2_76L
 G1_R_2P_F028_h39_25P75L_1HR_R1_76L
 G1_R_2P_F028_h39_25P75L_1HR_R2_76L

Handrail variations

G1_R_2P_F028_h34_25P75L_OHR_R1_76L
 G1_R_2P_F028_h34_25P75L_OHR_R2_76L
 G1_R_2P_F028_h34_25P75L_1W_R1_76L
 G1_R_2P_F028_h34_25P75L_1W_R2_76L
 G1_R_2P_F028_h39_25P75L_1W_R1_76L
 G1_R_2P_F028_h39_25P75L_1W_R2_76L

0 Piers

G1_R_0P_F028_h27_25C75L_2HR_R1_76L
 G1_R_0P_F028_h39_25C75L_2HR_R1_76L

Lab Delft

Hydraulic conditions, bridge deck at 27 cm

N1_R_2P_F013_h22_25P75L_1HR_R1_76
 N1_R_2P_F013_h22_25P75L_1HR_R2_76
 N1_R_2P_F013_h22_25P75L_1HR_R3_76
 N1_R_2P_F013_h27_25P75L_1HR_R1_76
 N1_R_2P_F013_h27_25P75L_1HR_R2_76
 N1_R_2P_F013_h33_25P75L_1HR_R1_76
 N1_R_2P_F021_h24_25P75L_1HR_R1_76
 N1_R_2P_F021_h24_25P75L_1HR_R2_76
 N1_R_2P_F013_h22_25C75L_1HR_R1_76
 N1_R_2P_F013_h27_25C75L_1HR_R1_76
 N1_R_2P_F013_h27_25C75L_1HR_R2_76
 N1_R_2P_F013_h33_25C75L_1HR_R1_76
 N1_R_2P_F013_h33_25C75L_1HR_R2_76
 N1_R_2P_F021_h22_25C75L_1HR_R1_76

Handrail configuration, bridge deck at 20 cm

Default: porous handrail

N1_R_2P_F015_h32_25P75L_1HR_deck20_R1_76L
 N1_R_2P_F015_h32_25P75L_1HR_deck20_R2_76L
 N1_R_2P_F015_h32_25P75L_1HR_deck20_R3_76L
 N1_R_2P_F015_h27,5_25P75L_1HR_deck20_R1_76L
 N1_R_2P_F015_h27,5_25P75L_1HR_deck20_R2_76L

N1_R_2P_F015_h27,5_25P75L_1HR_deck20_R3_76L

No handrail

N1_R_2P_F015_h27,5_25P75L_OHR_deck20_R1_69,67L

N1_R_2P_F015_h27,5_25P75L_OHR_deck20_R2_76L

N1_R_2P_F015_h27,5_25P75L_OHR_deck20_R3_76L

N1_R_2P_F015_h30_25P75L_OHR_deck20_R1_76L

Solid wall

N1_R_2P_F015_h32_25P75L_1W_deck20_R1_76L

N1_R_2P_F015_h32_25P75L_1W_deck20_R2_76L

N1_R_2P_F015_h32_25P75L_1W_deck20_R3_76L

N1_R_2P_F015_h27,5_25P75L_1W_deck20_R1_76L

N1_R_2P_F015_h27,5_25P75L_1W_deck20_R2_76L

N1_R_2P_F015_h27,5_25P75L_1W_deck20_R3_76L

N1_R_2P_F015_h27,5_25P75L_1W_deck20_R4_76L

Solid wall and rounded deck

N1_R_2P_F015_h32_25P75L_1RW_deck20_R1_76L

N1_R_2P_F015_h32_25P75L_1RW_deck20_R2_76L

N1_R_2P_F015_h32_25P75L_1RW_deck20_R3_76L

N1_R_2P_F015_h27,5_25P75L_1RW_deck20_R1_76L

N1_R_2P_F015_h27,5_25P75L_1RW_deck20_R2_76L

N1_R_2P_F015_h27,5_25P75L_1RW_deck20_R3_76L

N1_R_2P_F015_h27,5_25P75L_1RW_deck20_R4_76L

N1_R_2P_F015_h27,5_25P75L_1RW_deck20_R5_76L

N1_R_2P_F015_h27,5_25P75L_1RW_deck20_R6_76L